8-2002

An Ecosystem Dynamics Model of Monterey Bay, California

Lawrence S. Klein

AN ECOSYSTEM DYNAMICS MODEL OF MONTEREY BAY, CALIFORNIA

By

Lawrence S. Klein

B.S. Middlebury College, 1998

A THESIS

Submitted in Partial Fulfillment of the

Requirements for the Degree of

Master of Science

(in Oceanography)

The Graduate School

The University of Maine

August, 2002

Advisory Committee:

Fei Chai, Associate Professor of Oceanography, Advisor

David Townsend, Professor of Oceanography, Director of S.M. S.

Huijie Xue, Associate Professor of Oceanography

James Wilson, Professor of Marine Sciences

AN ECOSYSTEM DYNAMICS MODEL OF MONTEREY BAY, CALIFORNIA

By Lawrence S. Klein

Thesis Advisor: Dr. Fei Chai

An Abstract of the Thesis Presented
in Partial Fulfillment of the Requirements for the
Degree of Master of Science
(in Oceanography)
August, 2002

Monterey Bay is an upwelling region with high biological productivity in the California Coastal Current System. Several moorings, developed and maintained by the Monterey Bay Aquarium Research Institute (MBARI), have produced a long-term, high-quality time series oceanographic data set for the Monterey Bay. The data set has revealed a more comprehensive picture of physical-biological interaction on seasonal and interannual variability.

To improve our understanding of how the marine ecosystem responds to physical forcing, especially upwelling, an open ocean ecosystem model was modified for the Monterey Bay upwelling region. The result was a nine-component ecosystem model of Monterey Bay, which produced simulated results comparable to the observations. The model included three nutrients (silicate, nitrate, and ammonia), two phytoplankton groups (small phytoplankton and diatoms), two zooplankton grazers (microzooplankton and mesozooplankton), and two detrital pools (silicon and nitrogen). The observed upwelling

velocity, nutrient concentrations at the base of the euphotic zone (40m), and solar radiation at the ocean surface were used to force the ecosystem model.

Through model and data comparison, as well as sensitivity studies testing ecosystem parameters, the model was capable of detailing the seasonal cycle of nutrient dynamics and phytoplankton productivity, as well as interannual variability, including El Niño Southern Oscillation (ENSO) impacts on biological productivity in the Monterey Bay.

ACKNOWLEDGEMENTS

My time spent at the University of Maine has been both academically and personally rewarding, thanks to those who have assisted me in my various endeavors. I extend my greatest gratitude to my advisor, Professor Fei Chai, for taking me on as his student, and giving me so many opportunities for new experiences. I have learned a great deal from his expertise.

I also thank my other committee members, Huijie Xue, Jim Wilson, and David Townsend, and special thanks to Lei Shi, as well as those who read my thesis drafts and offered me constructive suggestions and guidance.

Finally, my appreciation and love go out to my family members, who despite living on the other coast, have always given me love, support, and advice throughout my academic career.

I would also like to acknowledge:

- Professor Fei Chai for research assistant funding
- Director/Professor David Townsend for graduate teaching assistant funding
- Maine Maritime Academy for academic funding
- Monterey Bay Aquarium Research Institute for the use of their resources
    - G.E. Friederich, F.P. Chavez, P.M. Waltz, R.P. Michisaki

TABLE OF CONTENTS

LIST OF TABLES

LIST OF FIGURES

Chapter 1

INTRODUCTION

Most of the seasonal upwelling that occurs along the Northeast Pacific Ocean margin is due to a combination of predominant northerly winds and offshore transport due to the Coriolis effect. This grouping of forces drives the upwelling system and is marked by nearshore surface waters migrating offshore with cold and deep, nutrient-rich, water rising to replace the surface water (Barber and Smith, 1981; Chelton et al., 1982; Brink, 1983; Huyer, 1983; Brink et al., 1995, Smith, 1995; Summerhayes et al., 1995; McGowan et al., 1996). The upwelled coastal water, sometimes occurring in bands alongshore that measure tens of kilometers wide, is remarkably nutrient-rich and capable of sustaining a bountiful upwelling fishery (Abbot and Zion, 1985; Kelly, 1985; Strub et al., 1991). Interests in better understanding coastal upwelling have resulted in large-scale oceanographic studies of these regions.

Monterey Bay is a region that has been the focus of oceanographic research for over three-quarters of a century. The bay has received ample scientific attention due to its unique open-ocean exposure sustaining higher biological productivity, large human population in the surrounding region, and complex bottom topography (steep submarine canyons measuring >1000m in depth). While research on coastal upwelling systems has been copious in the past, it has only been over the last decade that new technology has enabled consistent, long-term time series data to be collected (Hutchings et al., 1995; Olivieri and Chavez, 2000). The Monterey Bay Aquarium Research Institute (MBARI) led the way with new technology. In 1989 MBARI began to establish and maintain time

series observations in the Monterey Bay that included biweekly cruises in addition to continuous data from multiple moored buoy "platforms" located around the bay (Chavez, 1996; Chavez, 1997) (Figure 1.1).

After the implementation of the Monterey Bay observation program, scientists have been able to use the data in order to gain insight into how biological and chemical systems respond to physical processes, such as wind, current, light, and temperature. The resulting information has greatly influenced the scientific community by creating a surge of continued research in Monterey Bay, as well as complementary research in other upwelling systems around the world.

Monterey Bay is a complex coastal environment. Upwelling occurs seasonally, driven by the Aleutian low-pressure system migrating northwest and the northwest high-pressure system shifting to the north in late winter. These atmospheric shifts are responsible for creating strengthened southward winds along the entire west coast of the United States (Strub et al. 1987a, b). As a result, Monterey Bay typically experiences high productivity during the spring and summer upwelling period when southward winds are prevalent, and low productivity during the non-upwelling winter season. Previous studies have characterized this pattern into three major oceanographic seasons: 1) "Upwelling," occurring during spring and summer, is characterized by increased northerly winds, southward surface flow, and episodic upwelling events; 2) "Oceanic," present from late summer through fall, is associated with continued southward surface flow, but with little to no wind driven upwelling events; and 3) The "Davidson" period, arising in the winter, is characterized by a northward surface flow without local

upwelling (Skogsberg, 1936; Skogsberg and Phelps, 1946, Pennington and Chavez, 2000).

The goal of this thesis was to create an ecosystem dynamics model for the Monterey Bay upwelling system in order to understand how biological and chemical systems respond to physical forcing on seasonal and interannual timescales. The nine-component ecosystem was developed by using Systems Thinking in an Experimental Learning Lab with Animation (STELLA). STELLA, a powerful computer program used for creating models of dynamic systems and processes, utilizes building block icons to construct a dynamic web of components (Appendix A.1.). Multiple model sensitivity runs can be conducted by using STELLA, providing the freedom to explore numerous scenarios within the model.

The model development and model experiments consisted of three main components. First, the seasonal cycle of nutrient dynamics and phytoplankton productivity was reconstructed in the model and compared with observations, and different physical forcing regimes were investigated. Second, a series of model sensitivity studies were conducted in order to gain insight into the model's internal dynamics. Third, the model ran over ten years (1990-2000) driven by observed upwelling velocities, subsurface nutrient concentrations, and surface light data in order to determine climate variability, such as El Niño and La Niña, effects on the biogeochemical cycle of Monterey Bay.

Ecosystem modeling approaches have been used widely in oceanographic research. A previous modeling study that has received much attention is the nitrogen-based, open-ocean ecosystem, model created by Fasham et al (1990). The model,

referred to as the "FDM" model, consisted of seven compartments: phytoplankton, zooplankton, bacteria, nitrate, ammonium, dissolved organic nitrogen (DON), and detritus. Originally designed to simulate the seasonal cycle near Bermuda, it has hence been extended to simulate seasonal cycles in the North Atlantic, equatorial Pacific, and most recently Monterey Bay, California (Sarmiento et al., 1993; Toggweiler and Carson, 1995; Olivieri and Chavez, 2000).

Olivieri and Chavez (2000) adapted Fasham et al's (1990) FDM model in order to simulate the Monterey Bay coastal upwelling ecosystem. The result was a seven-box model, driven by upwelling velocity, photosynthetically active radiation (PAR), and changes in the mixed layer depth, that was capable of reproducing nitrate concentration, primary productivity, and phytoplankton biomass.

Chai et al (2002) successfully created a one-dimensional ecosystem model for the equatorial Pacific upwelling system. The model consisted of ten components (nitrate, silicate, ammonium, small phytoplankton, diatoms, microzooplankton and meso-zooplankton, detrital nitrogen and silicon, and total CO_2) and was forced by area-averaged annual mean upwelling velocity and vertical diffusivity (mixing). The model was capable of reproducing the high nitrate, low chlorophyll, and low silicate (HNLCLS) conditions in the equatorial Pacific.

Other scientists have developed and used similar models to study upwelling systems in the Monterey Bay and elsewhere. However, by adapting Chai et al's (2002) model design, this study has added more complexity to the seven-component ecosystem model by differentiating between two types of phytoplankton (small phytoplankton [less than 5μm in diameter, excluding diatoms] and diatoms) as well as two types of

zooplankton (microzooplankton and mesozooplankton). The zooplankton classes were not differentiated by size, but by growth rate and feeding preference. These components will be further discussed in the model description section in chapter two.

By only utilizing seven components, previous models have lacked not only the ability to add detail to the spring bloom dynamics, but also the capability to address different nutrient cycles (i.e., nitrogen vs. silicon) (Fasham et al., 1990; Olivieri and Chavez, 2000). With two additional components, this study, hereafter referred to as the nine-component model, provides further detail and insight into which primary producer contributes most significantly to a spring bloom, as well as to the seasonality of phytoplankton productivity. The nine-component model is also capable of determining which zooplankton group grazes the phytoplankton population and terminates the bloom.

Another subjacent motivation for creating the ecosystem model using STELLA was to utilize a hands-on, non-language-programming modeling package to determine whether the nine-component model was capable of processing the highly complex marine dynamics of Monterey Bay. The benefits of using such a modeling package include reduced modeling time, more user-friendly design template, and most importantly, the introduction of modeling to non-programming scientists and the general public.

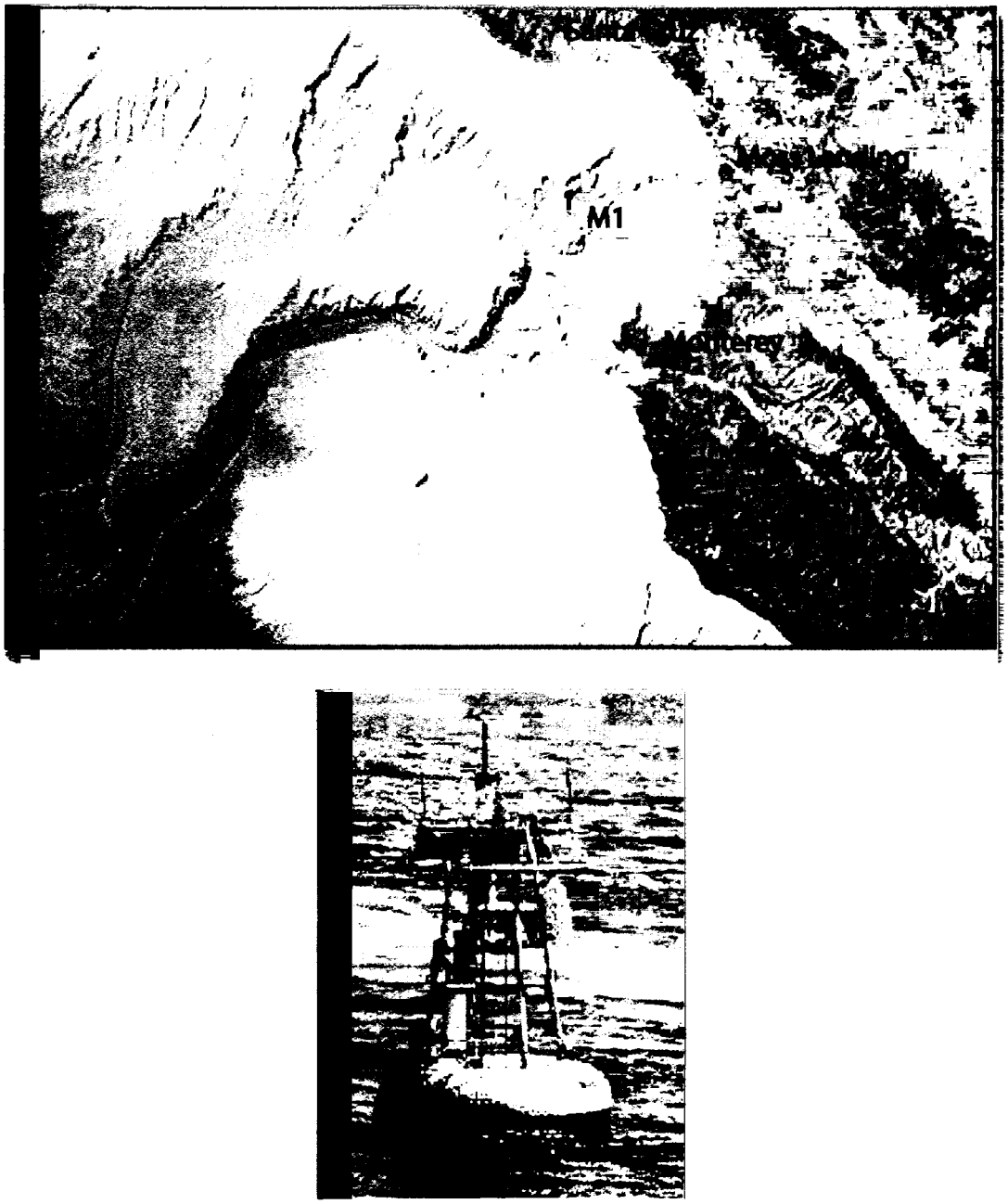

(images modified from http://mbari.org/data/mapping/mapping.htm, http://www.mbari.org/bog/Projects/MOOS/)

Figure 1.1: Top- Bottom bathymetry image of Monterey Bay's submarine canyons. Bottom- An image of the M1 mooring platform *in situ*.

Chapter 2

METHODS

The Model

This thesis hybridized two previous modeling endeavors by incorporating the ten-component model framework adapted from Chai et al's (2002) equatorial Pacific upwelling model and Olivieri and Chavez's (2000) seven-component model of Monterey Bay, hereafter referred to as the O&C model (2000) (Figure 2.1, 2.2).

Chai et al's (2002) ten-component ecosystem model, originally developed for the equatorial Pacific, is capable of reproducing high nitrate, low chlorophyll, low silicate (HNLCLS) conditions. The adapted model used nine of the ten components, consisting of two forms of dissolved inorganic nitrogen: nitrate and ammonium (NO_3 and NH_4), detrital nitrogen and silicon (DN and DSi), dissolved silicic acid (silicate= $Si(OH)_4$), two sizes of phytoplankton: small phytoplankton cells (S1) (< 5 μm in diameter) and diatoms (S2) (> 5 μm in diameter), and microzooplankton and mesozooplankton (Z1 and Z2) (size classification broken down by growth rate and feeding preference).

S1 represents small phytoplankton (< 5 μm), whose biomass is primarily grazed down by microzooplankton (Z1). Most of S1's daily net productivity is remineralized (Chavez et al., 1991; Murray et al., 1994; Landry et al., 1997; Chai et al., 2002). S2 represents larger phytoplankton (> 5 μm) strictly composed of diatoms. It is responsible for strong phytoplankton blooms and disproportionately contributes to sinking flux in the

form of ungrazed production or large fecal pellets (Smetacek, 1985; Wefer, 1989; Peinert et al., 1989; Bidigare and Ondrusek, 1996; Chai et al., 2002).

Z1 represents microzooplankton and has a growth rate similar to S1 and a grazing rate that is dependent upon its density (Landry et al., 1997). Z2 represents a larger grazer, mesozooplankton, whose grazing preferences consist of S2 and detrital nitrogen (DN). Z2 is also the primary predator of Z1. Z2 zooplankton have defined feeding thresholds and complex grazing dynamics (Frost and Franzen, 1992).

The detrital pool was divided between detrital nitrogen (DN) and detrital silicon (DSi), with detrital silicon (DSi) having a faster sinking rate than detrital nitrogen (DN) (Chai et al., 2002).

Based on the compiled MBARI data set, the nine-component model was configured for the M1 mooring located in Monterey Bay at approximately 36.747°N, 122.022°W (Figure 1.1). Because the model's nine components were averaged from surface to 40 meters depth at the M1 mooring, it is considered to be spatially zero-dimensional (often referred to as a "box-model").

The Equations

The nine-component model was divided into two main sections, physical and biological. The physics of the system relates to upwelling velocity and photosynthetically active radiation (PAR). The biology element represents all of the different sources and sinks from a specific biological compartment. All of the nine-component model equations take on the form:

$$\frac{\partial N_i}{\partial t} = PHYSICS(N_i) + BIOLOGY(N_i) \qquad i = 1,.....,9 \tag{1}$$

where N_i represents the concentration of a specific compartment (For example, N_1=NO_3, N_2= NH_4, etc).

The term PHYSICS(N_i) represents the concentration change due to physical processes such as upwelling and advection. In the model, the physical terms only affect the nitrate and silicate compartments. For compartments other than nitrate and silicate, it is assumed that physical processes will not change the concentration of an individual compartment.

The physical terms, PHYSICS(N_i), for the nine-component model are:

$$PHYSICS(N_i) = \underbrace{w\frac{BN_i - N_i}{H}}_{\text{advection}} + \underbrace{\frac{BN_i - N_i}{T}}_{\text{mixing}} \tag{1B}$$

w = Upwelling velocity

N_i = Nutrient concentration in mixing layer (N_1= NO_3, N_2= $Si(OH)_4$)

BN_i = Advected nutrient concentration (BN_1= observed NO_3 at 40m, BN_2= observed $Si(OH)_4$ at 40m)

H = Depth from surface to 40m below surface

T = 30 days (amount of time it takes to recover from disturbance)

The biological terms, BIOLOGY(N_i), for the nine-component model are:

$$BIOLOGY(NO_3) = \quad -NPS1 \qquad -(NPS2 - RPS2) \tag{2}$$

NO_3 uptake by $S1$ $\quad$ NO_3 uptake by $S2$

$NPS1$ = NO_3 uptake by small phytoplankton

$NPS2$ = $Si(OH)_4$ uptake by diatoms

$RPS2$ = NH_4 uptake by diatoms

Note: Nitrate is used by both small phytoplankton (S1) and diatoms (S2). The total nitrogen requirement for diatoms are from two parts, NH_4 and NO_3. NH_4 uptake by diatoms, RPS2, is calculated directly (see equation 14). Assuming the Si:N uptake ratio by diatoms is 1:1, then the rest of the nitrogen required by diatoms is from the nitrate pool, which is: NPS2-RPS2. NPS2 represents silicate uptake by diatoms (see equation 13).

$$BIOLOGY(Si(OH)_4) = \quad -NPS2 \qquad +\gamma_5 DSI \tag{3}$$

$Si(OH)_4$ uptake by $S2$ $\quad$ Si dissolution from DSI

γ_5 = 0.0 day^{-1} (biogenic silica dissolution rate)

$$BIOLOGY(NH_4) = \quad -RPS1 \qquad -RPS2 \qquad +reg_1 Z1 + reg_2 Z2 \tag{4}$$

NH_4 uptake by $S1$ $\quad$ NH_4 uptake by S2 $\quad$ NH_4 regeneration

$RPS1$ = Regenerated production of small phytoplankton

reg_1 = 0.22 day^{-1} (microzooplankton excretion rate of ammonium)

reg_2 = 0.1 day^{-1} (mesozooplankton excretion rate of ammonium)

$$BIOLOGY(S1) = +(NPS1 + RPS1) \quad - G_1 \quad - \gamma_4 S1^2 \tag{5}$$

total production by *S1* grazing by *Z1* mortality

γ_4 = 1.5 day^{-1} (small phytoplankton specific mortality rate)

$$BIOLOGY(S2) = +2NPS2 \quad - 2G_2 \quad - 2\frac{(w_1 S2)}{H} \quad - 2\gamma_3 S2^4 \tag{6}$$

production by *S2* grazing by *Z2* sinking mortality

w_1 = 3.0 m day^{-1} (diatom sinking speed)

γ_3 = 0.085 day^{-1} (diatom specific mortality rate)

Note: all the source and sink terms are counted twice for diatom growth in order to reflect both nitrogen and silicon uptake by diatoms, silicon to nitrogen ratio is 1:1 in diatoms (Brzezinski, 1985), the uptake silicon to nitrogen ratio by diatoms is also 1 (Leynaert et al., 2001). We do not allow silicon to nitrogen ratio in diatoms change in the current model.

$$BIOLOGY(Z1) = \quad + G_1 \quad - G_3 \quad - reg_1 Z1 \tag{7}$$

grazing on *S1* predation by *Z2* NH_4 reg.

$$BIOLOGY(Z2) = +(G_2 + G_3 + G_4) \; - (1-\gamma_1)(G_2 + G_3 + G_4) \; - reg_2 Z2 \; - \gamma_2 Z2^2 \tag{8}$$

grazing by *Z2* detritus-N prod. NH_4 reg. Loss

γ_1 = 0.75 (mesozooplankton assimilation efficiency on Z1 and DN)

γ_2 = 0.05 (mmol m^{-3}) $^{-1}$ day^{-1} (mesozooplankton specific mortality rate)

Note: the fecal pellet production of silicate by Z2 equals to the grazing on diatoms by Z2, which is G_2, two terms cancel each other in the equation (8). In this sense, the Z2 component just passes the silicate from the diatoms directly to the detritus-Si pool. G_3 is predation term on Z1 by Z2. G_4 is grazing term on DN by Z2.

$$BIOLOGY(DN) = +(1-\gamma_1)(G_2 + G_3 + G_4) \quad - G_4 \quad - \frac{(w_2 DN)}{H} \quad + \gamma_3 S2^4 \qquad (9)$$

detritus-N prod. grazing by *Z2* sinking S2 mortality

w_2 = 10.0 m day^{-1} (detritus nitrogen sinking speed)

$$BIOLOGY(DSI) = +G_2 \quad - \frac{(w_3 DSI)}{H} \quad - \gamma_5 DSI \quad + \gamma_3 S2^4 \qquad (10)$$

detritus-Si prod. Sinking Si dissolution S2 mortality

w_3 = 2.0 * w_2 = 20.0 m day^{-1} (detritus silicon sinking speed)

Growth (NPS1, RPS1, NPS2, and RPS2) and grazing (G_1, G_2, G_3, and G_4) functions are expressed next along with the values for each parameters used in the calculations. NPS1 is the nitrate uptake rate by small phytoplankton:

$$NPS1 = \mu 1_{max} \frac{NO_3}{K_{NO_3} + NO_3} \quad e^{-\psi NH_4} \quad \left(1 - e^{-\frac{\alpha}{\mu 1_{max}} I}\right) S1 \tag{11}$$

NO_3 uptake by $S1$ = NO_3 regulation NH_4 inhibition light regulation

$\mu 1_{max}$ = 2.8 day^{-1} (maximum specific growth rate of small phytoplankton)

ψ = 5.6 (mmol m^{-3})$^{-1}$ (ammonium inhibition parameter)

K_{NO3} = 0.75 mmol m^{-3} (half-saturation for nitrate uptake by S1)

α = 0.033 (W m^{-2})$^{-1}$ day^{-1} (initial slope of P-I curve)

I is the irradiance, and is derived from 2 years (late 1998-early 2000) of MBARI daily averaged PAR (Wm^{-2}) values. I is depth averaged down to the bottom of the euphotic zone (40m). A ten-day running average was then applied to the time series. The resulting time series was then averaged into a one-year time series.

RPS1 is the ammonium uptake rate by small phytoplankton:

$$RPS1 = \mu 1_{max} \frac{NH_4}{K_{NH_4} + NH_4} \quad \left(1 - e^{-\frac{\alpha}{\mu 1_{max}} I}\right) S1 \tag{12}$$

NH_4 uptake by $S1$ = NH_4 regulation light regulation

K_{NH4} = 0.5 mmol m^{-3} (half-saturation for ammonium uptake by S1)

NPS2 is the silicate uptake rate by diatoms:

$$NPS2 = \mu 2_{max} \frac{Si(OH)_4}{K_{Si(OH)_4} + Si(OH)_4} \quad \left(1 - e^{-\frac{\alpha}{\mu 2_{max}} I}\right) S2 \tag{13}$$

$Si(OH)_4$ uptake by $S2$ = $Si(OH)_4$ regulation light regulation

$\mu 2_{max}$ = 1.5 day^{-1} (maximum specific growth rate of diatoms)

$K_{si(OH)4}$ = 4.0 mmol m^{-3} (half-saturation for silicate uptake by S2)

RPS2 is the ammonium uptake rate by diatoms:

$$RPS2 = \mu 2_{max} \frac{NH_4}{K_{S2-NH_4} + NH_4} \left(1 - e^{-\frac{\alpha}{\mu 2_{max}} I}\right) S2 \qquad (14)$$

NH_4 uptake by $S2$ = NH_4 regulation light regulation

$K_{S2\text{-}NH4}$ = 0.5 mmol m^{-3} (half-saturation for ammonium uptake by diatoms)

G_1 is the microzooplankton grazing rate on small phytoplankton:

$$G_1 = G1_{max} \frac{S1}{K1_{gr} + S1} * Z1 \qquad (15)$$

food limitation

$G1_{max}$ = 1.0 day^{-1} (microzooplankton maximum growth rate)

$K1_{gr}$ = 0.75 mmol m^{-3} (half-saturation for microzooplankton ingestion)

G_2, G_3, and G_4 are the mesozooplankton grazing rates on diatoms, microzooplankton, and detrital nitrogen, respectively:

$$G_2 = G2_{\max} \frac{\zeta_1 S2}{K2_{gr} + \zeta_1 S2 + \zeta_2 Z1 + \zeta_3 DN} Z2 \quad (16)$$

$$G_3 = G2_{\max} \frac{\zeta_1 Z1}{K2_{gr} + \zeta_1 S2 + \zeta_2 Z1 + \zeta_3 DN} Z2 \quad (17)$$

$$G_4 = G2_{\max} \frac{\zeta_1 DN}{K2_{gr} + \zeta_1 S2 + \zeta_2 Z1 + \zeta_3 DN} Z2 \quad (18)$$

$G2_{max}$ = 0.45 day^{-1} (mesozooplankton maximum growth rate)

$K2_{gr}$ = 1.0 mmol m^{-3} (half-saturation for mesozooplankton ingestion)

where ζ_1, ζ_2 and ζ_3 are the preferences for a given food type, and defined as following:

$$\zeta_1 = \frac{\rho_1 S2}{\rho_1 S2 + \rho_2 Z1 + \rho_3 DN}$$
$$\zeta_2 = \frac{\rho_2 Z1}{\rho_1 S2 + \rho_2 Z1 + \rho_3 DN} \quad (19)$$
$$\zeta_3 = \frac{\rho_3 DN}{\rho_1 S2 + \rho_2 Z1 + \rho_3 DN}$$

ρ_1 = 0.60, ρ_2 = 0.20, ρ_3 = 0.20

All parameters used in the standard experiment are presented in Table 2.1.

The Data

All seasonal cycle data used in the model was collected from the website and archives of MBARI (http://www.mbari.org/bog/NOPP/data.htm). Interannual data also

Table 2.1: Model Parameters.

Parameters	Symbol	9-comp. value	Chai et al. value	Unit
Light attenuation due to water	k_1	0.1	0.046	m^{-1}
Light attenuation by phytoplankton	k_2	0.03	0.03	m^{-1} (mmol m^{-3})$^{-1}$
Initial slope of P-I curve	α	0.033	0.025	day^{-1} (W m^{-2})$^{-1}$
Maximum specific growth rate of small phytoplankton	$\mu 1_{max}$	2.8	2.0	day^{-1}
Maximum specific diatom growth rate	$\mu 2_{max}$	1.5	3.0	day^{-1}
Ammonium inhibition parameter	ψ	5.6	5.59	(mmol m^{-3})$^{-1}$
Half-saturation for nitrate uptake	K_{NO3}	0.75	0.5	mmol m^{-3}
Half-saturation for ammonium uptake by small phytoplankton	K_{NH4}	0.5	0.05	mmol m^{-3}
Half-saturation for silicate uptake	$K_{Si(OH)4}$	4.0	3.0	mmol m^{-3}
Half-saturation for ammonium uptake by diatoms	$K_{S2\text{-}NH4}$	0.5	1.0	mmol m^{-3}
Half-saturation for microzooplankton ingestion	$K1_{gr}$	0.75	0.5	mmol m^{-3}
Half-saturation for mesozooplankton ingestion	$K2_{gr}$	1.0	0.25	mmol m^{-3}
Depth from surface to base of thermocline	H	40	n/a	m
Microzooplankton excretion rate to ammonium	reg_1	0.22	0.2	day^{-1}
Mesozooplankton excretion rate to ammonium	reg_2	0.1	0.1	day^{-1}
Microzooplankton maximum grazing rate	$G1_{max}$	1.0	1.35	day^{-1}
Mesozooplankton maximum grazing rate	$G2_{max}$	0.45	0.53	day^{-1}
Mesozooplankton assimilation efficiency	γ_1	0.75	0.75	
Mesozooplankton specific mortality rate	γ_2	0.05	0.05	day^{-1}
Diatom specific mortality rate	γ_3	0.085	0.05	day^{-1}
Small phytoplankton specific mortality rate	γ_4	1.5	n/a	day^{-1}
Biogenic silica dissolution rate	γ_5	0.0	0.0	day^{-1}
Grazing preference for diatoms	ρ_1	0.6	0.7	
Grazing preference for microzooplankton	ρ_2	0.2	0.2	
Grazing preference for detritus	ρ_3	0.2	0.1	
Diatoms sinking speed	w_1	3.0	1.0	m day^{-1}
Detrital N sinking speed	w_2	10	10	m day^{-1}
Detrital Si sinking speed	w_3	20	20	m day^{-1}

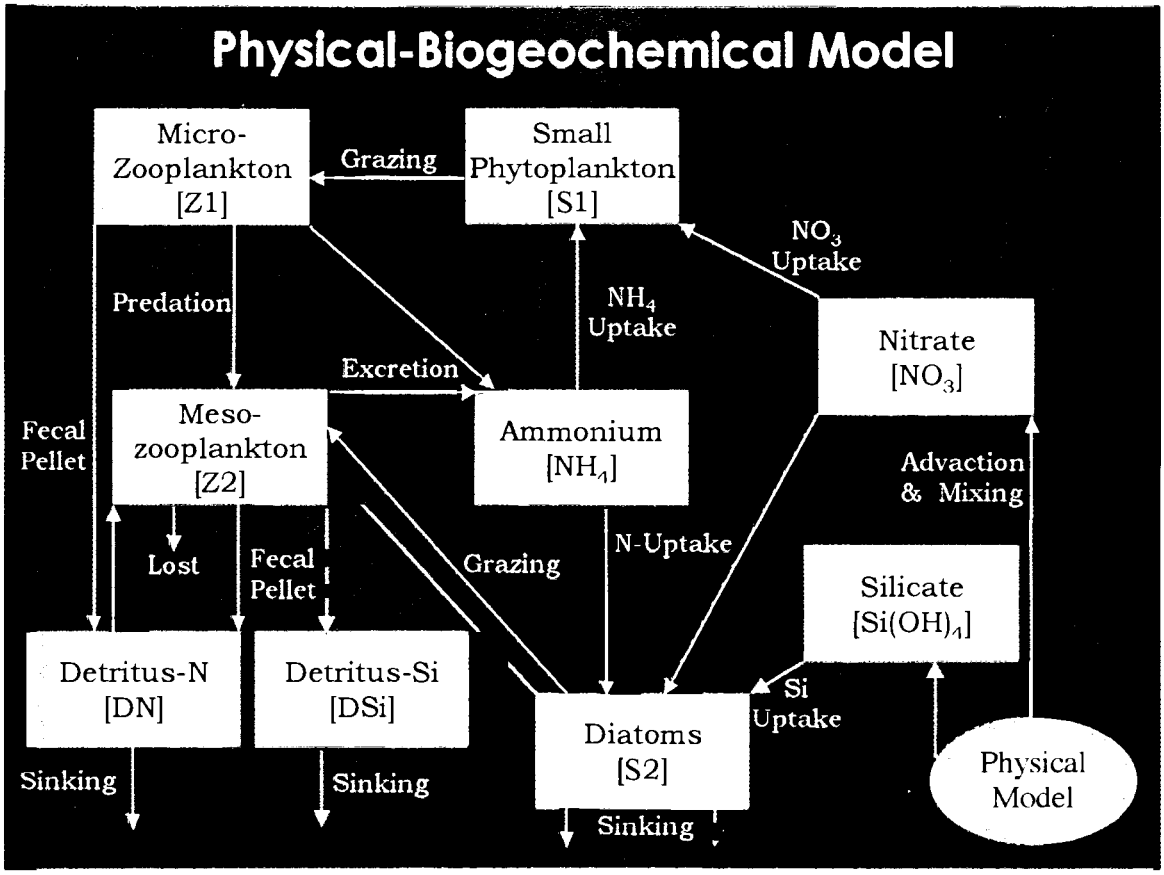

(modified from Chai et al., 2002)

Figure 2.1: A schematic diagram of the upper-ocean physical-biogeochemical model. A white line indicates the flow of nitrogen, while a red line indicates the flow of silicon.

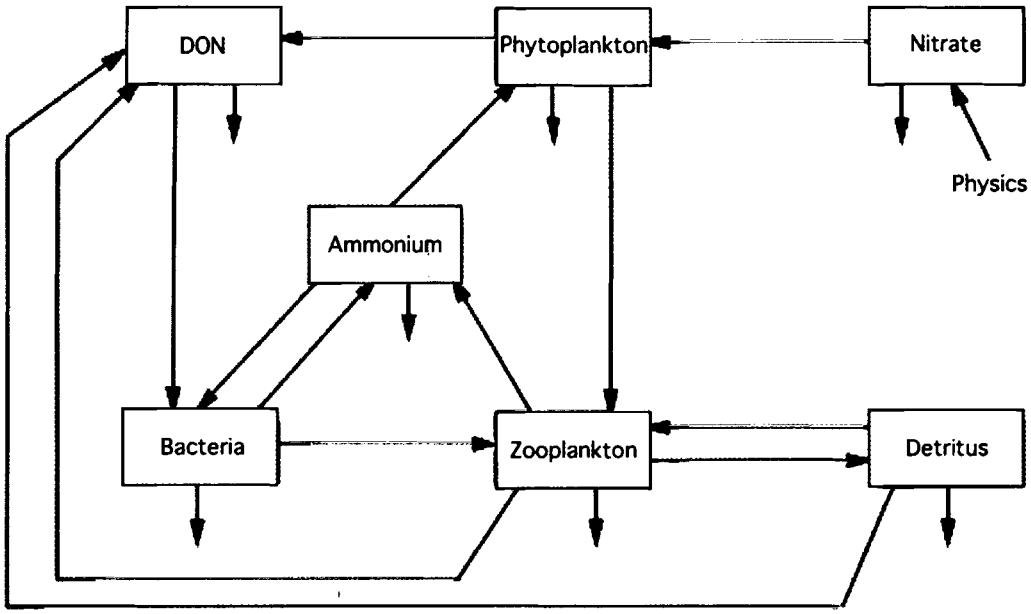

Figure 2.2: Olivieri and Chavez's (2000) seven-box model of the planktonic food web used to represent the Monterey Bay ecosystem.

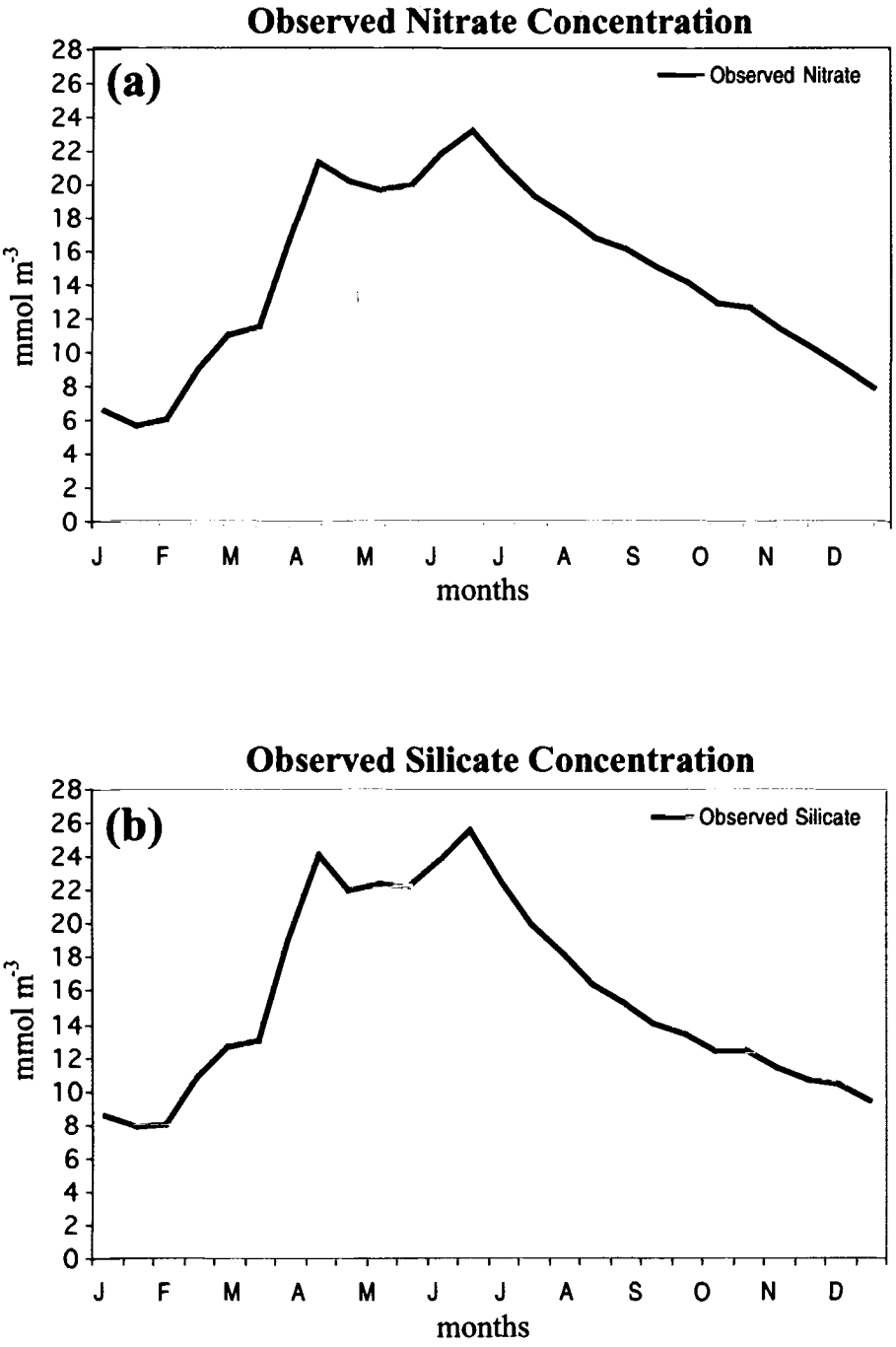

Figure 2.3: Monterey Bay observed biweekly seasonal nitrate and silicate values at 40m.

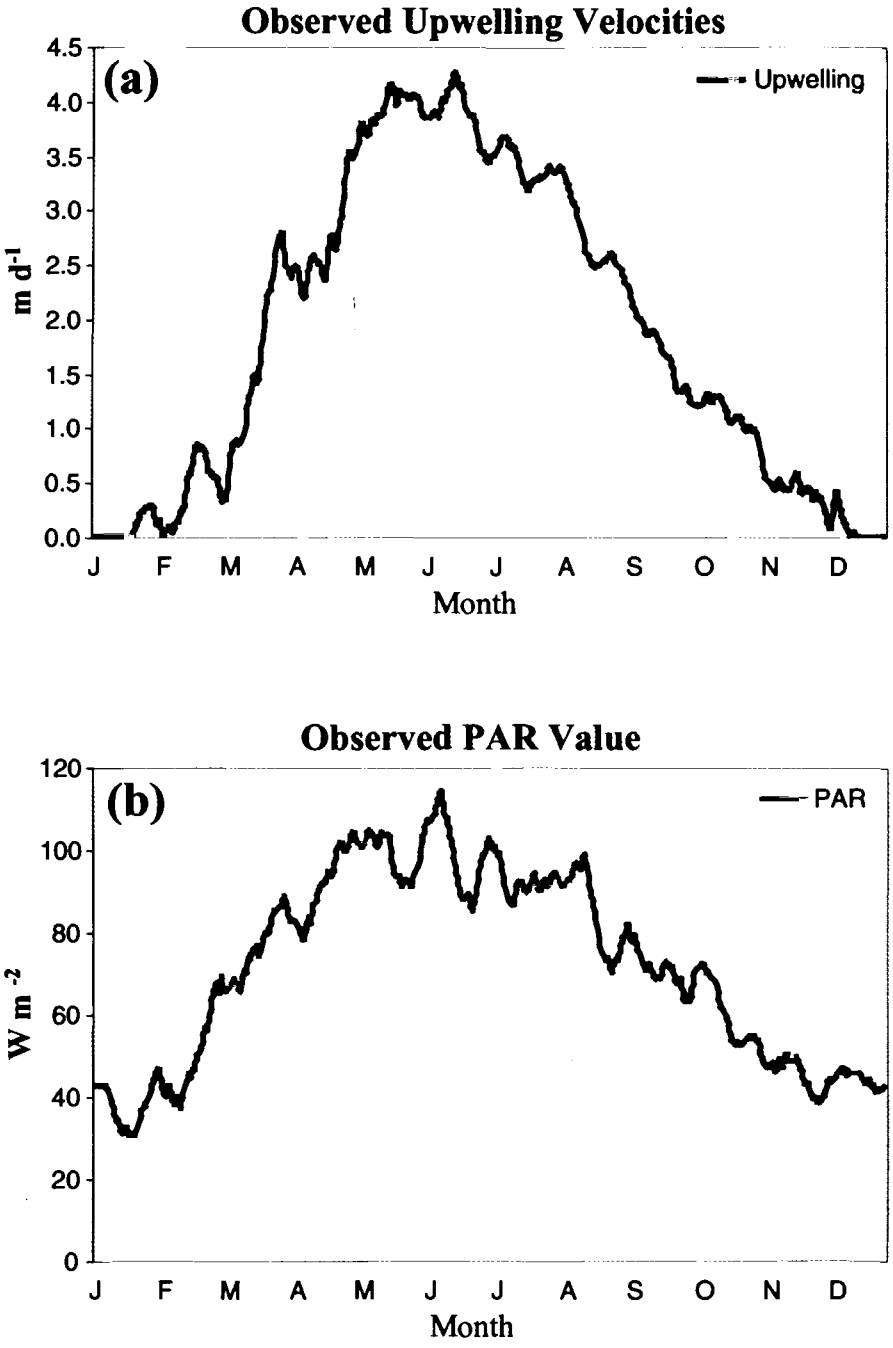

Figure 2.4: Observed, ten-day smoothed, seasonal upwelling velocities and photosynthetically active radiation (PAR) values from a twelve-year average from Monterey Bay.

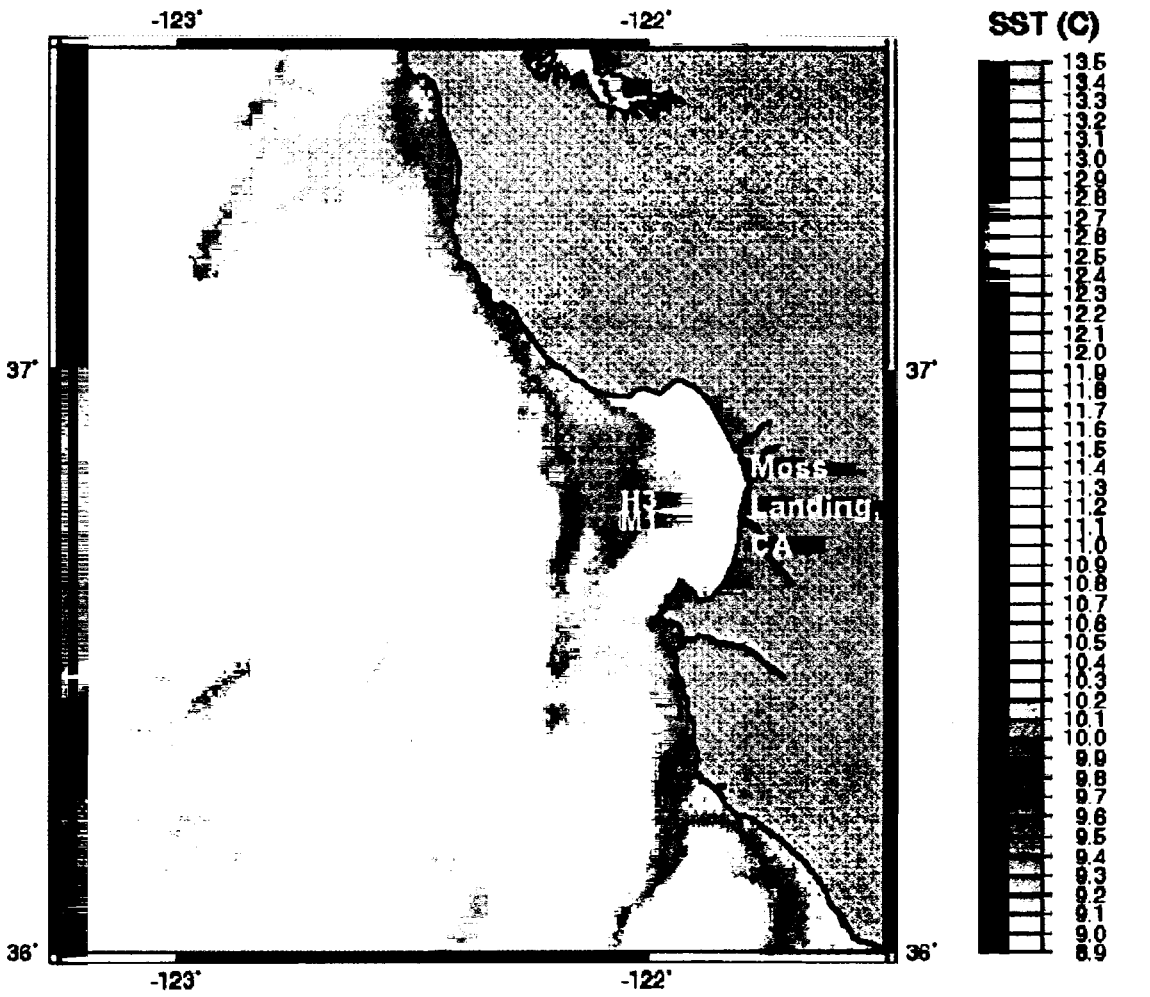

(modified from Olivieri and Chavez, 2000)

Figure 2.5: Sea surface temperature of the Monterey Bay region during the upwelling season of 1995.

Chapter 3

SEASONAL CYCLE AND SENSITIVITY STUDIES

Model Evolution

The model, developed originally for the equatorial Pacific upwelling system, was not initially suitable for the Monterey Bay region. As a result, several parameters in the model needed to be adjusted for the Monterey Bay environment. Some model equations, including diatom mortality, were also not adjusted for the Monterey Bay. Using sensitivity studies incrementally, each of these factors was honed to reflect an accurate simulation bounded by measured values.

Modifications to the nine-component model included adjusting the growth rates, half-saturation concentrations of nutrient uptake, and zooplankton food preferences. Some of the larger modifications were the nutrient advection and mixing terms, and the three mortality terms.

The nutrient advection term was upwelling velocity multiplied by a nutrient concentration at 40 meters depth. In order to maintain conservation of water mass, upwelled water exits from the compartment with lower nutrient concentrations than when it entered (see advection term in equation 1B). The second modification was to adapt a mixing term with a relaxation time (T) of 30 days, which represents nutrient mixing processes between the top of the compartment and the water below (0-40m depth) (see mixing term in equation 1B). The result was a more stable model that produced very accurate simulation values.

The mortality terms, which were initially simply based upon linear or second-order loss terms, were modified into quadratic and, in the case of the diatom mortality function, quartic functions (equations 5,9,10). These adaptations removed high-frequency oscillations that plagued early results and further aided the stability and accuracy of the nine-component model (Table 3.1).

Nitrate, Ammonium, and Silicate

In the nine-component model, the two forms of nitrogen that S1 and S2 procured were nitrate (NO_3) and ammonium (NH_4). NH_4 and NO_3 were used primarily based upon availability and phytoplankton preference. Both NH_4 and NH_4 -uptake maintained high values in the winter and low in the summer, while NO_3 and NO_3-uptake were greatest in the summer and dwindled in the winter months. Both NH_4 and NO_3 concentrations and utilization pattern match with the seasonal upwelling regimes of Monterey Bay (Pennington and Chavez, 2000). NH_4, recycled from zooplankton excretion, was primarily utilized during the winter months, representing regenerated production, while NO_3 values were particularly low due to lack of upwelling in the winter. During the spring and summer upwelling months, however, NO_3 concentration was high and, hence, saturated phytoplankton uptake of NO_3.

The modeled NO_3 values compared well with observed values throughout the entire year (Table 3.2). Maximum values were over 14 mmol m^{-3} and occurred in late June (Figure 3.1a). In contrast, NH_4 values were at a maximum in the winter months

(Davidson period) with values around 0.5 mmol m^{-3}. While this NH_4 value compared well with O&C's modeled results, the annual mean value for both models was considerably lower than the observed values (Table 3.2). The primary reasons for this inconsistency are the fact that ammonium turnover time is short, the regeneration of ammonium is a very difficult process to study, and there are very few observed data sets with which to compare the modeled results.

In addition to nitrogen requirements, diatoms uptake silicate ($Si(OH)_4$) in order to construct their siliceous frustules (cell walls). Modeled concentrations of $Si(OH)_4$, while slightly lower throughout the season, compared well with observed values. The overall seasonal mean was within range of the observed value (Figure 3.1b) (Table 3.1). The maximum value of $Si(OH)_4$, reached in late June, was 22 mmol m^{-3}. Similar to nitrate concentration, silicate concentration values were lowest during the Davidson period. The nitrate and silicate concentrations and their seasonality were directly linked to the changes of upwelling velocities. Without upwelling, the nutrient-rich, bottom water would never reach the surface. The nutrient levels were at a minimum during the Davidson period due to a lack of upwelling during the winter. It was not until the upwelling favorable seasons of spring and summer that advective processes brought the deep, nutrient replete, coastal California waters to the surface. Due to the overwhelming supply of nutrients, phytoplankton growth was saturated with excessive nutrients, therefore, the upwelled nutrients ended up increasing the concentrations in the surface.

Primary Production, Phytoplankton, Chlorophyll, and f-ratio

Observed primary productivity (PP) minimum and maximum values followed the same seasonal pattern as the nutrients, with a winter minimum of 0.5 g C m^{-2} d^{-1} and a late spring, early summer maximum exceeding 2.5 g C m^{-2} d^{-1} (Figure 3.2b).

The modeled annual mean PP model values were extremely similar to the mean observed PP values from mooring M1, as well as to the O&C annual averaged PP model estimates (Table 3.1). PP was calculated based upon the uptake rate of nitrate and ammonium by S1 and uptake of silicate by S2. A conversion factor was used in the calculation of PP; this conversion includes the depth-average from the surface down to 40m, the Redfield ratio of C:N (6.625), and a mol:gC conversion factor (12). Primary production, including the conversion factor, were calculated using the following equation,

$$PP = 40 * 6.625 * 12(\mathrm{NPS1} + \mathrm{RPS1} + \mathrm{NPS2}) \qquad (20)$$

Because diatoms take up nitrate and silicate in a 1:1 ratio, NPS2 was used in the equation to represent total nitrogen uptake by diatoms.

The modeled annual primary production had slightly lower values before and after the upwelling season. Winter values were approximately 0.5 g C m^{-2} d^{-1}, dropping slightly between year days (YD) 1 and 20, and then rapidly increasing with the onset of upwelling intensification and light increase. PP reached a maximum of 2.45 g C m^{-2} d^{-1} during the peak of the upwelling season in May and June. Following the decrease in

upwelling values, PP began to taper off in August, the beginning of the "oceanic" period (Figure 3.2b).

The annual mean of phytoplankton biomass was 1.26 mmol N m^{-3}, and compared well with the observed value of 1.64 mmol N m^{-3}. It should be noted that the chlorophyll *a*: C conversion is widely variable, ranging from .01 to .1 (Geider et al., 1997; Taylor et al., 1997). Based upon the environment of Monterey Bay, a mass ratio of .02, or 1:50, was used in the conversion of the observed value from mg Chl *a* to mmol N (equation 21).

Observed chlorophyll (Chl) values were retrieved directly from the MBARI website and a 40m depth average was applied to the retrieved data. Observed Chl values, again following the seasonal trend, reached a winter minimum of 0.75 mg m^{-3} and a late spring, early summer maximum of 3.0 mg m^{-3} (Figure 3.2a).

The modeled Chl values were derived from combined phytoplankton (P= S1+S2) values of small phytoplankton and diatoms, in nitrogen unit, using a gram-chlorophyll to mole-nitrogen ratio of 1.59. This ratio corresponds to a chlorophyll-to-carbon mass ratio of 1:50 and a C:N ratio of 6.625. Carbon has an atomic mass of 12, hence making the conversion equation,

$$Chl = P\left(\frac{6.625 * 12}{50}\right), \text{ or simplified, } Chl = P\,(1.59) \qquad (21)$$

The nine-component model produced a Chl level of 1.36 mg m^{-3} at the beginning of the year. These values quickly increased following the onset of the upwelling season and increase of light to values around 2.5 mg m^{-3}, and stayed at relatively high values

until the beginning of the "oceanic" period, in August, when it began, once again, to taper back to its winter values (Figure 3.2a).

The nine-component model is also capable of differentiating between "new" and "regenerated" production (Dugdale and Goering, 1967). New production (N_n) is comprised of small phytoplankton uptake of nitrate (NPS1) and diatom uptake of nitrate, while regenerated production (N_r) is calculated as ammonium uptake by both phytoplankton groups. The *f*-ratio is defined as the ratio of new to total production and can be written,

$$f - \text{ratio} = \frac{N_n}{N_n + N_r} \tag{22}$$

The calculated value is in the range between zero (all regenerated production) and one (all new production), depicting relative amounts of new (NO_3) and regenerated (NH_4) nutrients (Eppley and Peterson, 1979). Modeled N_r uptake was low to moderate and relatively constant for the duration of the year. N_n increased as a function of upwelling, with maximum *f*-ratio values of .81 in March and April (Figure 3.3). The new production increased with the onset of the upwelling period as nutrients were brought up from the nutrient replete bottom waters. New production was also boosted during the spring and summer seasons due to increased light levels in the form of enhanced availability of light and longer days, which in turn augmented phytoplankton photosynthetic processes.

Zooplankton Biomass and Grazing

The nine-component modeled zooplankton biomass was around 0.55 mmol N m^{-3} in the winter, increasing as phytoplankton biomass production increased until reaching stable values of approximately 1.3 mmol N m^{-3}.

Olivieri and Chavez (2000) discussed experiments carried out by Silver and Davoll (1975, 1976, 1977) for which zooplankton samples were collected at a station a few kilometers north of the mooring platform M1. The Silver and Davoll (1975, 1976, 1977) zooplankton biomass values were initially recorded in displacement volumes (ml 1000 m^{-3}) and converted by Olivieri and Chavez (2000) to mmol N m^{-3}. The values calculated in this model study were approximately half those of Olivieri and Chavez's (2000), but within range of Monterey Bay observed zooplankton values (Table 3.2). However, it must be mentioned again that due to the lack of studies in zooplankton dynamics in this region there are uncertainties associated with the conversions used.

Nine-component modeled zooplankton had an annual mean grazing rate of 0.18 mmol N m^{-3} d^{-1}. This value was less than half that of the O&C model, 0.50 mmol N m^{-3} d^{-1}, but between the two observed values of 0.48 mmol N m^{-3} d^{-1} from the Peru upwelling system (Dagg et al., 1980) and 0.11 mmol N m^{-3} d^{-1} from the Benguela Current (Stuart, 1986). It is difficult, however, to compare zooplankton grazing rates between the two models because the nine-component model's grazers subsisted on small phytoplankton, diatoms, and detritus, while the O&C model dealt with only one size-class for phytoplankton, bacteria, and detritus.

Seasonal Cycle and Sensitivity Studies

Utilizing one set of parameters in the model, as outlined in the methods section and Table 2.1, the seasonal cycle produced by the model is defined as the "control" run. This control run provides a basis for comparison for a series of sensitivity analyses. Along with the nine-component model's four forcing mechanisms, light (PAR), upwelling velocity, and two nutrient values (NO_3 and $Si(OH)_4$), the model is comprised of 25 parameters. Six sensitivity studies were performed trying to understand the factors controlling the seasonal cycle, each with an independent parameter modification. All concentration values used for the sensitivity studies were based upon averaged spring bloom values for May. A detailed list and description of the studies can be referenced in Table 3.3.

Sensitivity study one was performed by consecutively substituting annual mean upwelling and PAR values for the model in order to test different forcing mechanisms. By combining upwelling velocity with nitrate and silicate concentrations, a single forcing term, "nutrient flux," was created ((NO_3 + $Si(OH)_4$)* Upwelling). The study consisted of four comparison runs: a control, annual mean nutrient flux (i.e, nitrate and silicate upwelling flux are constant throughout the year), annual mean PAR (i.e., light is constant for the entire year), and a combination of annual mean nutrient flux and annual mean PAR (both nutrient fluxes and light are constant for the entire year) (Table 3.3) (Figures 3.4, 3.5).

Both nutrient terms responded similarly to the annual mean nutrient flux substitution. As expected, NO_3 and $Si(OH)_4$ values became much higher during the winter (approximately 9 and 14 mmol m^{-3} for nitrate and silicate, respectively), and lower

during the spring and summer (approximately 5 and 11 mmol m^{-3}) (Table 3.1) (Figure 3.4). Because the annual mean nutrient flux during winter was greater than the control values, there was greater nutrient input. In the summer, however, upwelling and nutrient values were lower than the control values. Diminishing seasonal variability in the nutrient flux resulted in reducing seasonal variability of the modeled nutrient concentrations. This suggests that the seasonal upwelling, along with the subsurface nutrient concentrations, controls surface nutrient concentrations in the Monterey Bay.

Using annual mean PAR, nutrient concentrations were slightly higher than the control runs during the spring and summer, and lower during the winter because increased light levels allow phytoplankton to photosynthesize and draw down the nutrients during the winter. The last study tested on the forcing mechanisms, a combination of annual mean nutrient flux and PAR, was conducted in order to confirm that the entire model would, in essence, "turn off" and remain constant if all driving forces were set to the annual mean values. The nutrient concentrations responded appropriately and remained constant throughout the season.

Stabilizing the driving forces created the same constant result for both chlorophyll and primary productivity (Table 3.1) (Figure 3.5). For the sensitivity study of annual mean nutrient flux, however, there was little variation from the constant value for either Chl or PP. Because the annual mean nutrient flux still provided enough nutrients, it did not affect phytoplankton productivity or modeled chlorophyll values significantly. On the other hand, in the case of annual mean PAR, both terms produced higher-than-average values in winter (1.5 mg m^{-3} and .75 g C m^{-3} d^{-1}, respectively) and lower-than-average in the spring and summer (2.2 mg m^{-3} and 1.4 g C m^{-3} d^{-1}). Because stabilizing

nutrient flux created little difference, while stabilizing PAR yielded large modifications in Chl and PP levels, one conclusion was that the phytoplankton productivity in the Monterey Bay might be light regulated. Further corroboration that the environment was light regulated can be seen in Table 3.1. Lower percent of both PP and Chl as compared to the base run, 33% and 23%, respectively, indicated that the seasonal variability of PP and Chl was indeed primarily light regulated.

Aside from testing different physical forcing mechanisms, a series of sensitivity studies was conducted by changing several key parameters in the model. Study two (the first parameter study) tested the effect of mesozooplankton grazing by varying the maximum grazing rate. It has been established for over a half a century that zooplankton grazing can control phytoplankton abundance (Riley, 1946, 1947; Chai et al., 1996). One model parameter that affects the zooplankton grazing efficiency is $G2_{max}$ (mesozooplankton maximum grazing rate, equation 16). $G2_{max}$ values were changed from 0.35-0.95 day^{-1} by increments of 0.05 day^{-1}up to 0.55 day^{-1}, after which the increment was 0.1 day^{-1}. The control used the value of 0.45 day^{-1}. By increasing the $G2_{max}$, both NO_3 and $Si(OH)_4$ slightly increased over the study period. In contrast, the diatom population, and primary production, plummeted (Figure 3.6a, b). The small phytoplankton population showed signs of a slow increase, attributed to the decrease in microzooplankton grazing pressure (Figure 3.6c). However, the PP values dropped significantly, due to the reduction of diatoms (Figure 3.6b). The mesozooplankton population increased sharply, following the increase in $G2_{max}$, but then reached a maximum and started a descent as its population began to outweigh its resources, mainly diatoms.

Study three, similar to study two, involved varying the microzooplankton maximum gazing rate. Chai et al. (1999 and 2002) documented and discussed the importance of zooplankton grazing in an equatorial ecosystem model. As the mesozooplankton sensitivity study showed, the importance of zooplankton grazing is also applicable to central California upwelling system. Another important grazing parameter that can be tested in the model is $G1_{max}$ (microzooplankton maximum grazing rate). $G1_{max}$ was changed from 0.9-2.25 day^{-1}, with values of 0.9, 0.95 1.0, 1.15, 1.25 day^{-1}, and henceforth up to 2.25 day^{-1} by increments of 0.25 day^{-1}. The value in the control run was 1.0 day^{-1}. As would be expected, there was insignificant variation in the modeled silicate concentration because microzooplankton biomass does not link directly with diatoms growth. Nitrate concentration increased slightly due to the decrease of small phytoplankton (Figure 3.7d). Small phytoplankton biomass was significantly depressed as microzooplankton grazing pressure increased (Figure 3.7c). The microzooplankton population, however, appeared to be controlled by a mirrored mesozooplankton population increase. The mesozooplankton increase also explains how the small phytoplankton population continued to decrease despite only a slight increase in microzooplankton grazing (Figure 3.7b). Diatoms were fractionally reduced due to the steady increase of the mesozooplankton population (Figure 3.7a). The variation of $G1_{max}$ was responsible for only slightly decreasing primary productivity because diatoms contribute a large percentage of total phytoplankton production.

The fourth study tested the value of $K_{Si(OH)4}$ (half-saturation for silicate uptake by diatoms) in order to investigate silicon dynamics. $K_{Si(OH)4}$ was changed from 0.5-14 mmol m^{-3}. The first and second values were 0.5 and 1.0 mmol m^{-3}, respectively. From

this point on, the values increased from 2.0-14 mmol m^{-3} by an increment of 2.0 mmol m^{-3} for each experiment. The silicate uptake half-saturation term showed to be a sensitive parameter in the silicon cycle. Upon increasing the $K_{Si(OH)4}$, the silicate concentration showed a relatively consistent increase, while diatoms showed a steady and significant population decrease (Figure 3.8a, d). $K_{Si(OH)4}$ controls the diatom growth rate. By increasing $K_{Si(OH)4}$, diatoms would grow slower and require more silicon, therefore resulting in higher silicate concentrations and lower diatom biomass. Even though the nitrate equivalent value, K_{NO3}, was not modified, nitrate concentration did show a slight, yet steady increase. This increase is an important example of how the nine-component model system is interconnected. The decrease in the diatom population affected a parallel decrease in the mesozooplankton population, because diatoms are the main diet source for mesozooplankton. In turn, the mesozooplankton population reduction allowed the microzooplankton population to grow and thereby increased grazing pressure upon the small phytoplankton population. The decrease in small phytoplankton resulted in the increase of the nitrate concentration. Because both diatoms and small phytoplankton populations were reduced significantly, primary productivity ebbed as well.

Taking advantage of the nine-component model's capability to distinguish between nitrate and ammonium as two separate nitrogen sources, new and regenerated production, the fifth study tested the effect of ammonium inhibition, ψ (ammonium inhibition parameter) in the nine-component model. The ammonium inhibition parameter is particularly important to the nine-component model since small phytoplankton preferentially use ammonium over nitrate (Dortch, 1990). The greater the ammonium inhibition parameter, the more the small phytoplankton will preferentially use ammonium

over nitrate. In order to determine the sensitivity of the ammonium inhibition parameter, ψ was varied from 0.7-12.6 (mmol $m^{-3})^{-1}$. The first increment of variation was 0.7 (mmol $m^{-3})^{-1}$, while the rest, from 1.4-12.6 (mmol $m^{-3})^{-1}$, were varied by increments of 1.4 (mmol $m^{-3})^{-1}$. Nitrate values responded positively to the increase in ψ value. With higher ψ values, small phytoplankton take up less nitrate, resulting in the increase of nitrate concentration. However, the response was not nearly as dramatic as the results found in Chai et al. (2002). This is primarily due to the fact that the Monterey Bay upwelling system with high nitrate concentration, compared to the lower nitrate concentration of the equatorial upwelling system, is less sensitive to ammonium inhibition. The small phytoplankton population decreased steadily except for a slight increase when the microzooplankton population crashed at approximately 8.4 (mmol $m^{-3})^{-1}$(Figure 3.9c). The mesozooplankton population remained relatively steady but began increasing shortly after the microzooplankton population collapse (Figure 3.9a). After the demise of the microzooplankton population, mesozooplankton subsisted strictly upon diatoms, its preferred foodsource, and to a lesser extent, detritus. Even after the microzooplankton's collapse, the small phytoplankton population began to diminish as well, owing to the effect of the ammonium inhibition parameter. Diatoms and silicate remained quite stable throughout the entire experiment, while PP slightly decreased (Figure 3.9a, c, b).

The sixth, and final, sensitivity study, examined α (initial slope of P-I curve) for silicate uptake by diatoms (NPS2) only. α for small phytoplankton uptake (NPS1) is unaltered. When α was changed from 0.013 to 0.053 (W $m^{-2})^{-1}$ day^{-1}, by an increment of 0.005 (W $m^{-2})^{-1}$ day^{-1}. The small phytoplankton population initially remained constant as the diatom population increased. Upon α reaching a value of 0.033 (W $m^{-2})^{-1}$ day^{-1}, both

phytoplankton populations began to increase steadily (Figure 3.10a, c). Microzooplankton's decrease throughout the study eased the grazing pressure upon the small phytoplankton, and thus allowed them to increase. The mesozooplankton biomass, which initially increased, began to level off towards higher α values. The mesozooplankton grazing pressure remained relatively low and constant throughout the test (Figure 3.10b). It was the PP values that steeply increased throughout the study, proving that both small phytoplankton and diatoms were prolific while the secondary producers remained relatively unproductive. Higher phytoplankton biomass reduced both nitrate and silicate concentration (Figure 3.10d).

Table 3.1: Comparison of different nine-component model runs.

Comparison Field	Nitrate ($mmolm^{-3}$)	Silicate ($mmolm^{-3}$)	PP ($gCm^{-2}d^{-1}$)	Chl (mgm^{-3})
Base Run (Control)				
Amplitude (Max-Min)	11.30 (14.77-3.47)	15.81 (21.95-6.14)	1.91 (2.48-.29)	2.19 (2.66-.97)
% of Base Run	100	100	100	100
Annual Mean Nutrient Flux				
Amplitude (Max-Min)	2.90 (8.72-5.82)	3.72 (14.37-10.65)	1.75 (2.13-.38)	1.43 (2.54-1.11)
% of Base Run	25.66	23.53	91.62	65.30
Annual Mean PAR				
Amplitude (Max-Min)	12.83 (15.14-2.31)	18.79 (22.79-4.0)	.64 (1.43-.80)	.52 (2.16-1.64)
% of Base Run	113.54	118.85	33.51	23.74
Annual Mean N.Flux & PAR				
Amplitude (Max-Min)	0 (7.47-7.47)	0 (12.38-12.38)	0 (1.24-1.24)	0 (2.04-2.04)
% of Base Run	0	0	0	0

Table 3.2: Annual mean values for the nine-component model, O&C (2000) model, and observed values from Monterey Bay.

Name	Units	Model	Observed	O&C Model	O&C Observed
Phytoplankton	mmol N m^{-3}	1.26	1.64[a]	3.78	2.61[aa]
Zooplankton	mmol N m^{-3}	0.95	0.56[b]	1.54	0.56[b]
Nitrate	mmol N m^{-3}	7.54	9.22[c]	3.24	4.10[d]
Ammonium	mmol N m^{-3}	0.14	0.49[d]	0.14	0.49[d]
Silicate	mmol N m^{-3}	12.72	15.82[c]	--	--
Detritus	mmol N m^{-3}	1.18	--	0.06	--
Primary Production	g C m^{-2} d^{-1}	1.31	1.30[e]	1.29	1.26[d]
Chlorophyll	mg m^{-2}	2.00	1.84[c]	--	--
Phytoplankton nitrate uptake	mmol NO_3 m^{-3} d^{-1}	0.19	--	1.48	0.79[f]
Phytoplankton silicate uptake	mmol $Si(OH)_4$ m^{-3} d^{-1}	0.31	--	--	--
Phytoplankton ammonium uptake	mmol NH_4 m^{-3} d^{-1}	0.11	--	0.23	0.23[g]
Zooplankton grazing phytoplankton	mmol N m^{-3} d^{-1}	0.18	--	0.50	0.48[h] 0.11[i]

[a] Mean value from Monterey Bay stations H3 and Mooring M1 and mmol N:mg:Chl a ratio of 1.59 (eqn. 21) (modified from Eppley et al., 1992)

[aa] Mean value from Monterey Bay stations H3 and Mooring M1 and mmol N:mg:Chl a ratio of 1 (Eppley et al., 1992)

[b] Acoustic estimated mean biomass for Monterey Bay (Chavez, unpublished)

[c] 40m weighted mean value from Monterey Bay mooring M1 (http://www.mbari.org/bog/NOPP/data.htm)

[d] Mean value from Monterey Bay stations H3 and mooring M1

[e] Mean integrated value from Monterey Bay mooring M1 (http://www.mbari.org/bog/NOPP/data.htm)

[f] ^{15}N uptakes and Model (Kudela and Chavez, 2000)

[g] ^{15}N uptakes from Monterey Bay (Kudela and Dugdale, 2000)

[h] From zooplankton mean biomass estimated with acoustics (Chavez unpublished) and a maximum consumption/biomass ratio of .86 d^{-1} for small copepods calculated from values for Peru upwelling system (Dagg et al., 1980)

[i] From zooplankton mean biomass estimated with acoustics (Chavez unpublished) and a maximum consumption/biomass ratio of .2 d^{-1} for euphausiids calculated of the Benguela Current (Stuart, 1986)

Table 3.3: Sensitivity study test list and descriptions.

Test Number	Parameter	Range	Figure Reference
1	Annual mean nutrient flux/PAR	n/a	3.4, 3.5
2	$G2_{max}$ (Mesozooplankton maximum grazing rate)	.35-.95	3.6
3	$G1_{max}$ (Microzooplankton maximum grazing rate)	.90-2.25	3.7
4	$K_{Si(OH)4}$ (Half-saturation for silicate uptake)	.5-14	3.8
5	ψ (Ammonium inhibition parameter)	.7-12.6	3.9
6	α (Initial slope of P-I curve)	.013-.053	3.10

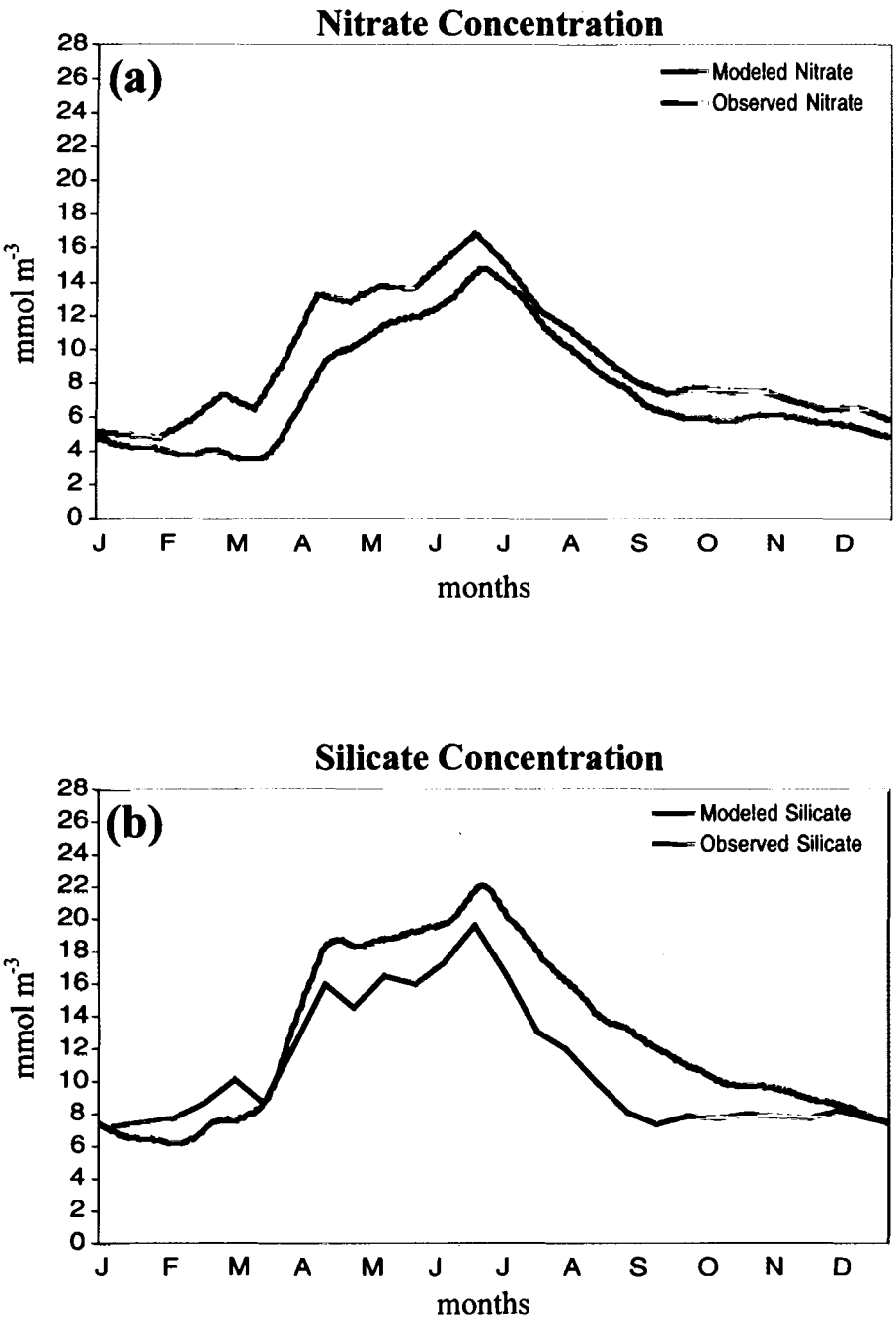

Figure 3.1: Seasonal Monterey Bay model results versus observed values of nitrate and silicate. Nitrate and silicate are the two nutrients that are the driving mechanism behind the nine-component model.

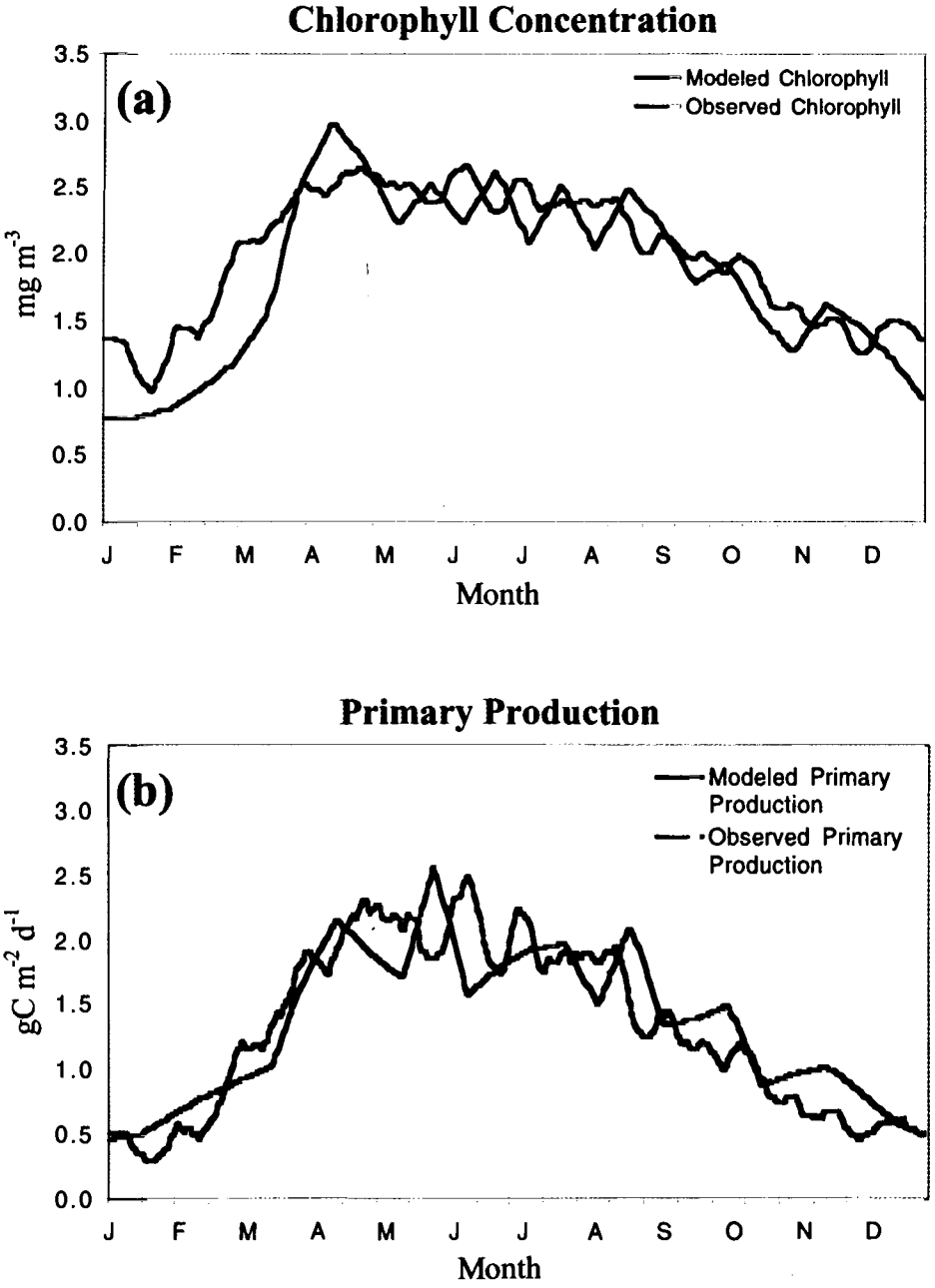

Figure 3.2: Chlorophyll and primary productivity modeled seasonal results as compared to observed Monterey Bay values.

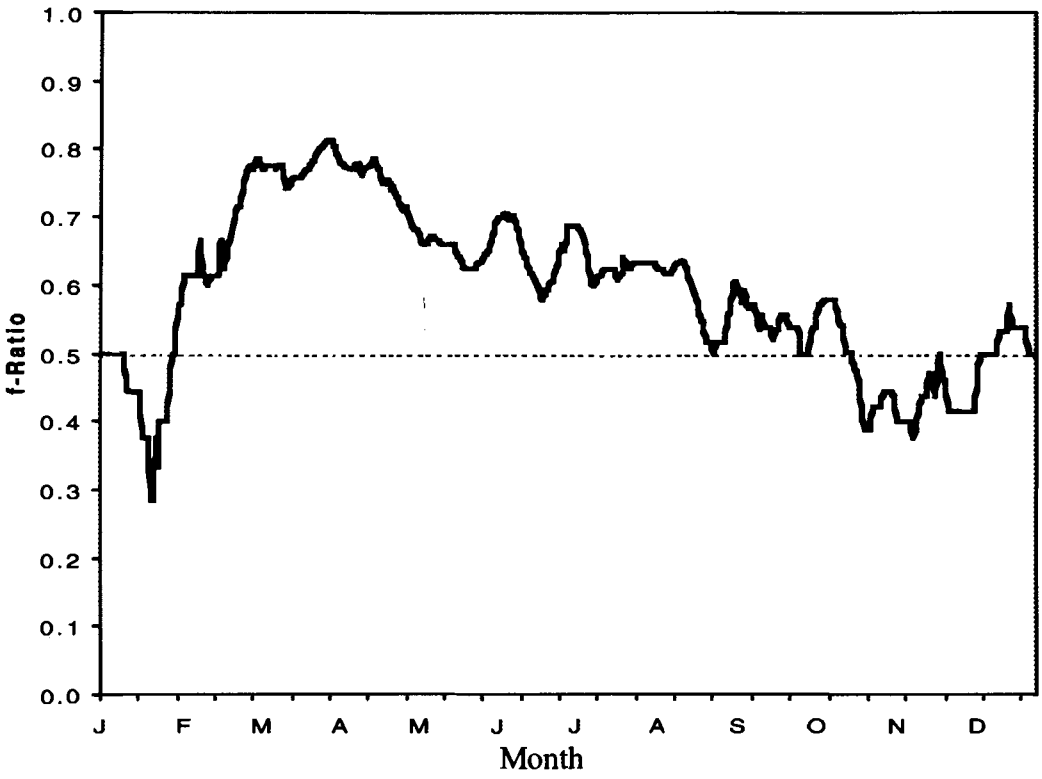

Figure 3.3: Annual cycle of *f*-ratio (ratio of new to total production) from the nine-component model. The dashed red line represents the division between new production (above 0.5) and regenerated production (below 0.5).

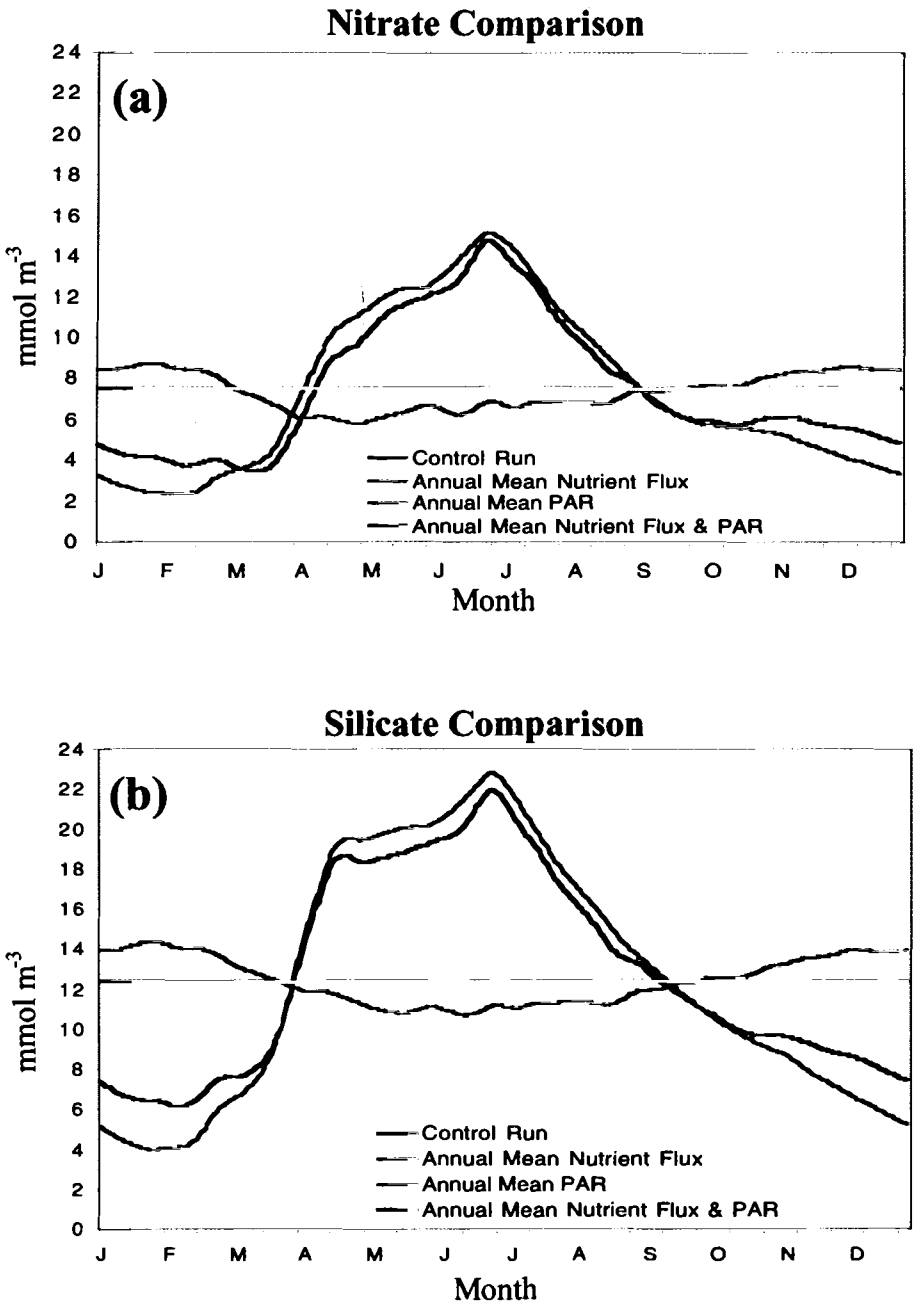

Figure 3.4: Sensitivity study runs of the seasonal model for nitrate and silicate. Each figure shows a control run (dark blue), a run with constant nutrient flux (green), a run with constant PAR (light blue), and a run where both nutrient flux and PAR are held constant throughout the season (red).

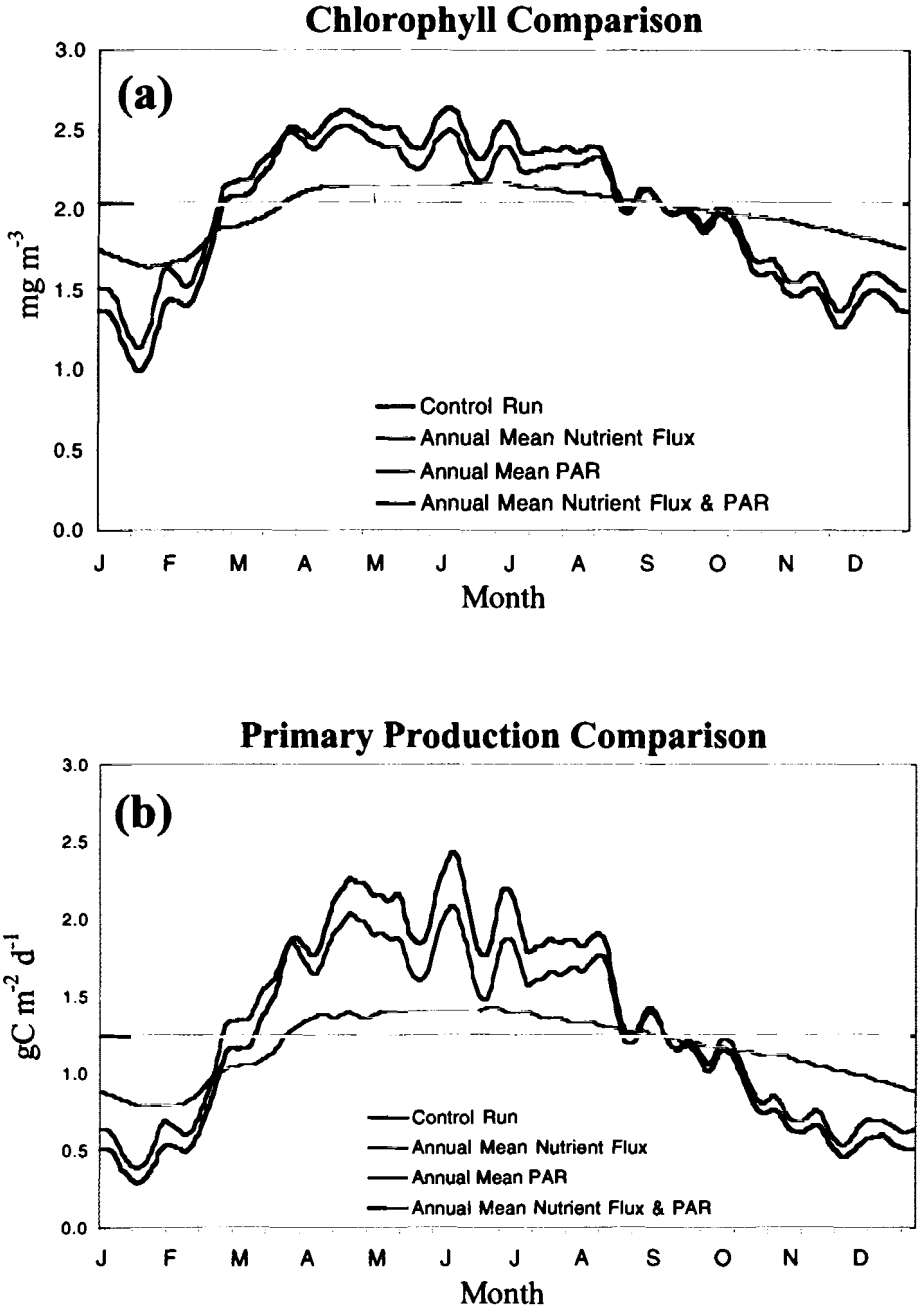

Figure 3.5: Sensitivity study runs of the seasonal model for chlorophyll and primary productivity. Each figure shows a control run (dark blue), a run with constant nutrient flux (green), a run with constant PAR (light blue), and a run where both nutrient flux and PAR are held constant throughout the season (red).

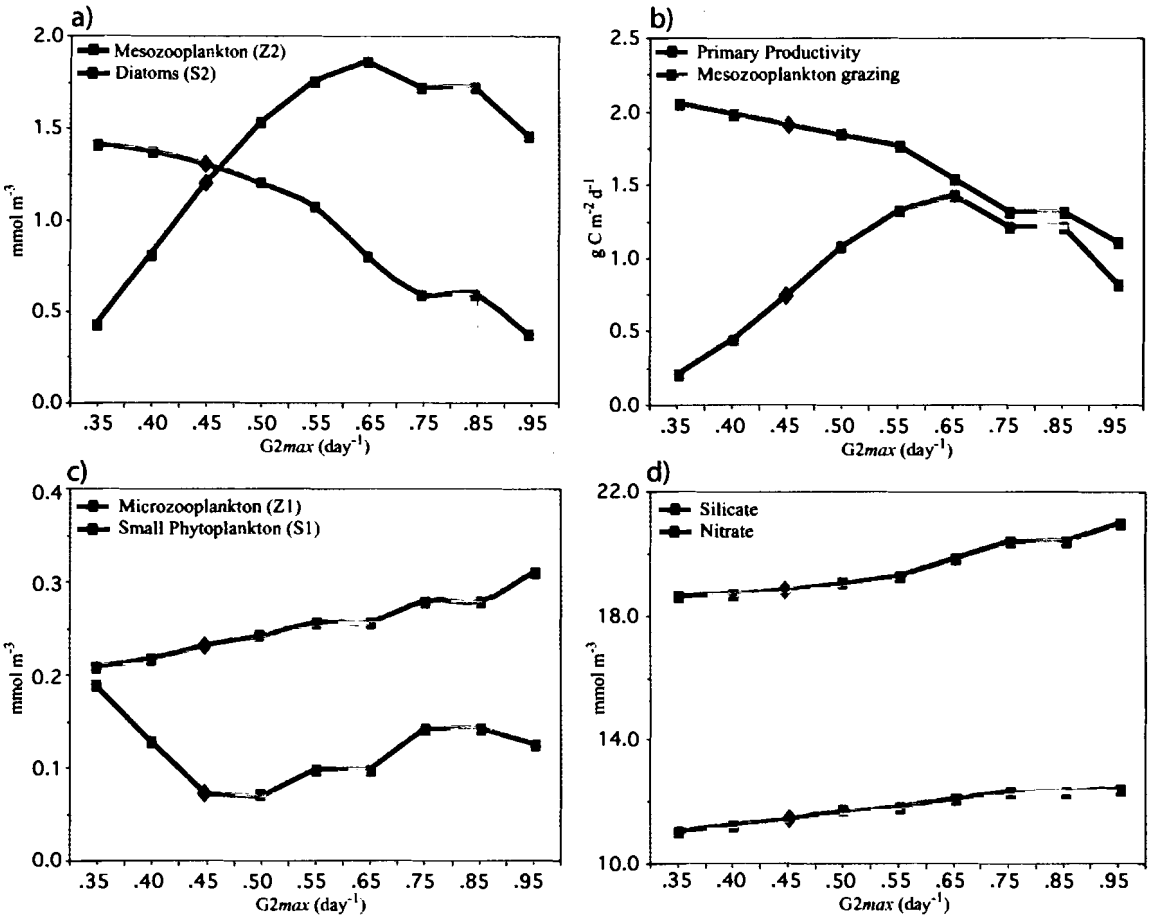

Figure 3.6: Response of several model components to changes in the parameter $G2_{max}$ (mesozooplankton maximum grazing rate). a) Mesozooplankton and Diatoms, b) Primary Productivity and Mesozooplankton grazing, c) Microzooplankton and Small Phytoplankton, d) Silicate and Nitrate. The control of the sensitivity study is indicated by a reverse colored diamond.

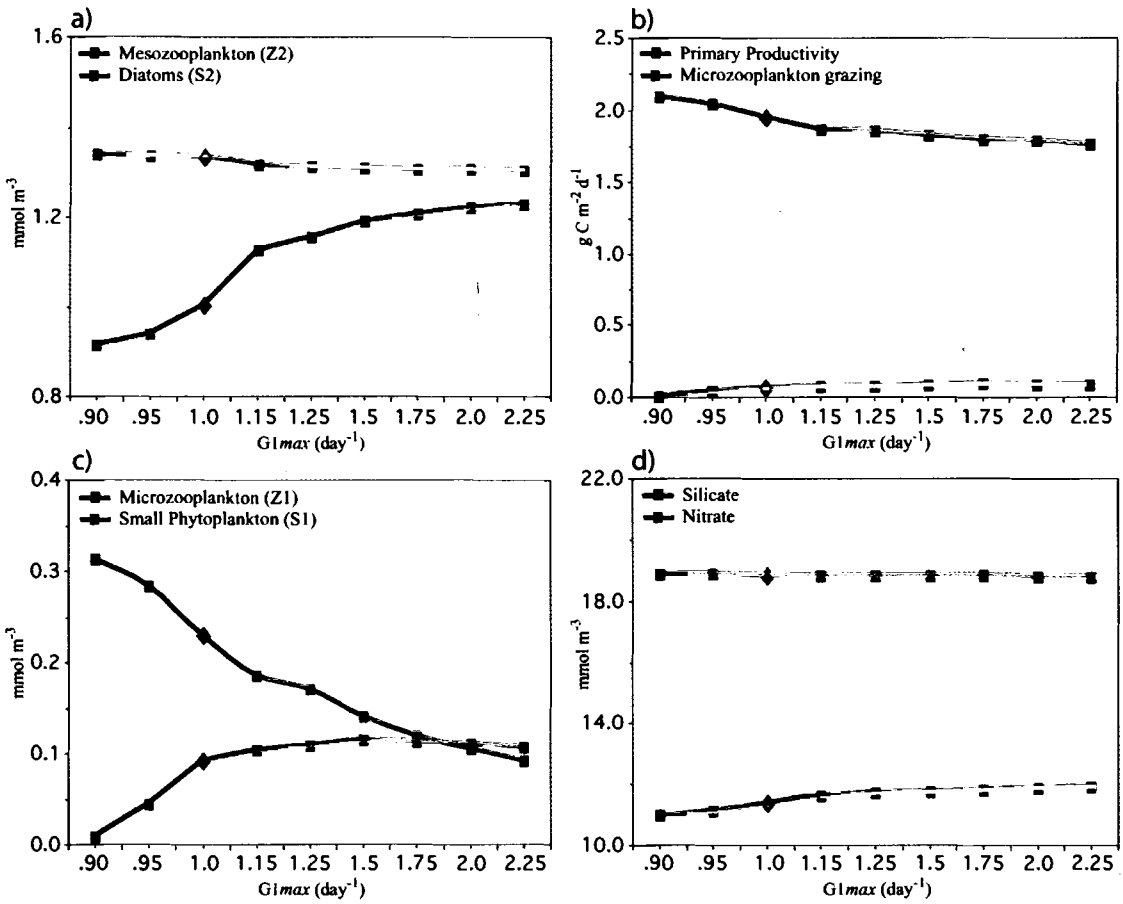

Figure 3.7: Response of several model components to changes in the parameter $G1_{max}$ (microzooplankton maximum grazing rate). a) Mesozooplankton and Diatoms, b) Primary Productivity and Microzooplankton grazing, c) Microzooplankton and Small Phytoplankton, d) Silicate and Nitrate. The control of the sensitivity study is indicated by a reverse colored diamond.

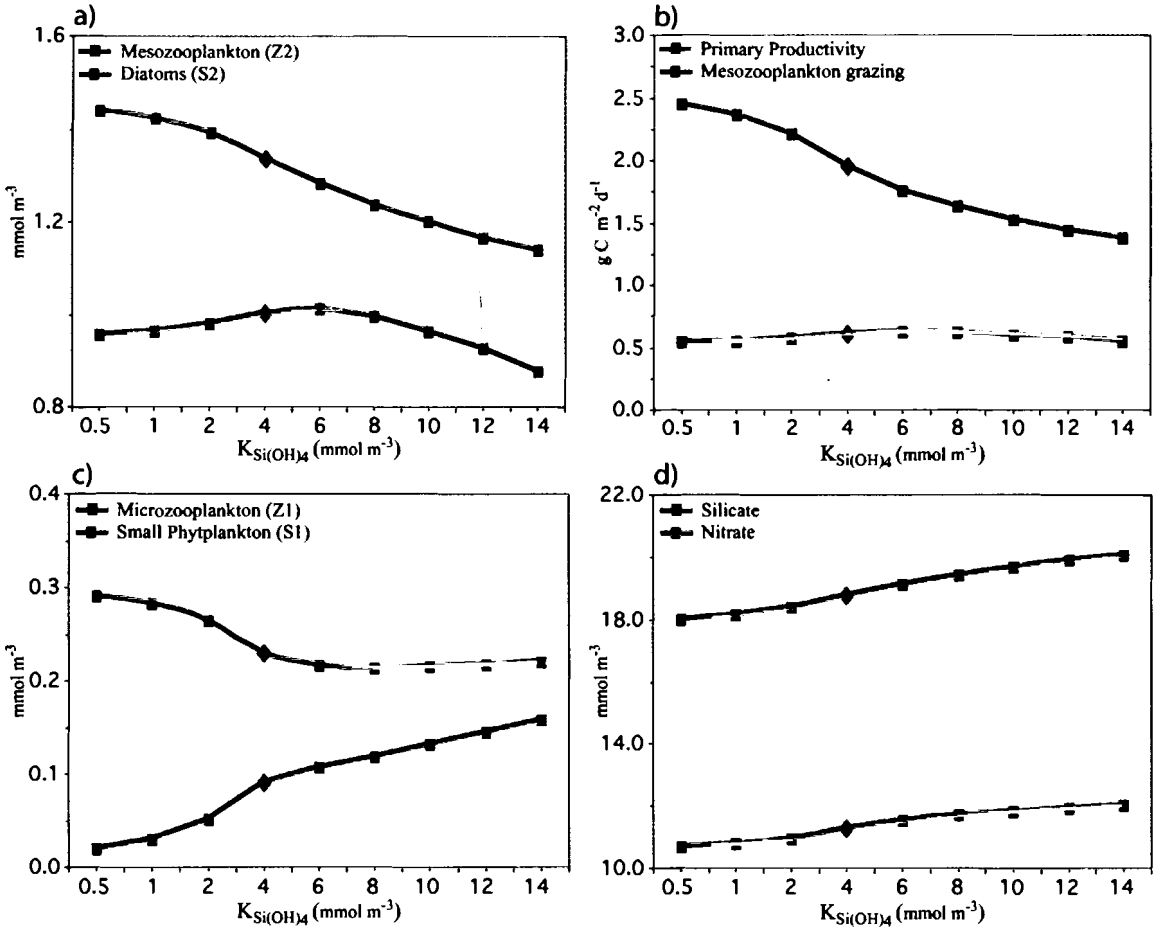

Figure 3.8: Response of several model components to changes in the parameter $K_{Si(OH)4}$ (half-saturation for silicate uptake). a) Mesozooplankton and Diatoms, b) Primary Productivity and Mesozooplankton grazing, c) Microzooplankton and Small Phytoplankton, d) Silicate and Nitrate. The control of the sensitivity study is indicated by a reverse colored diamond.

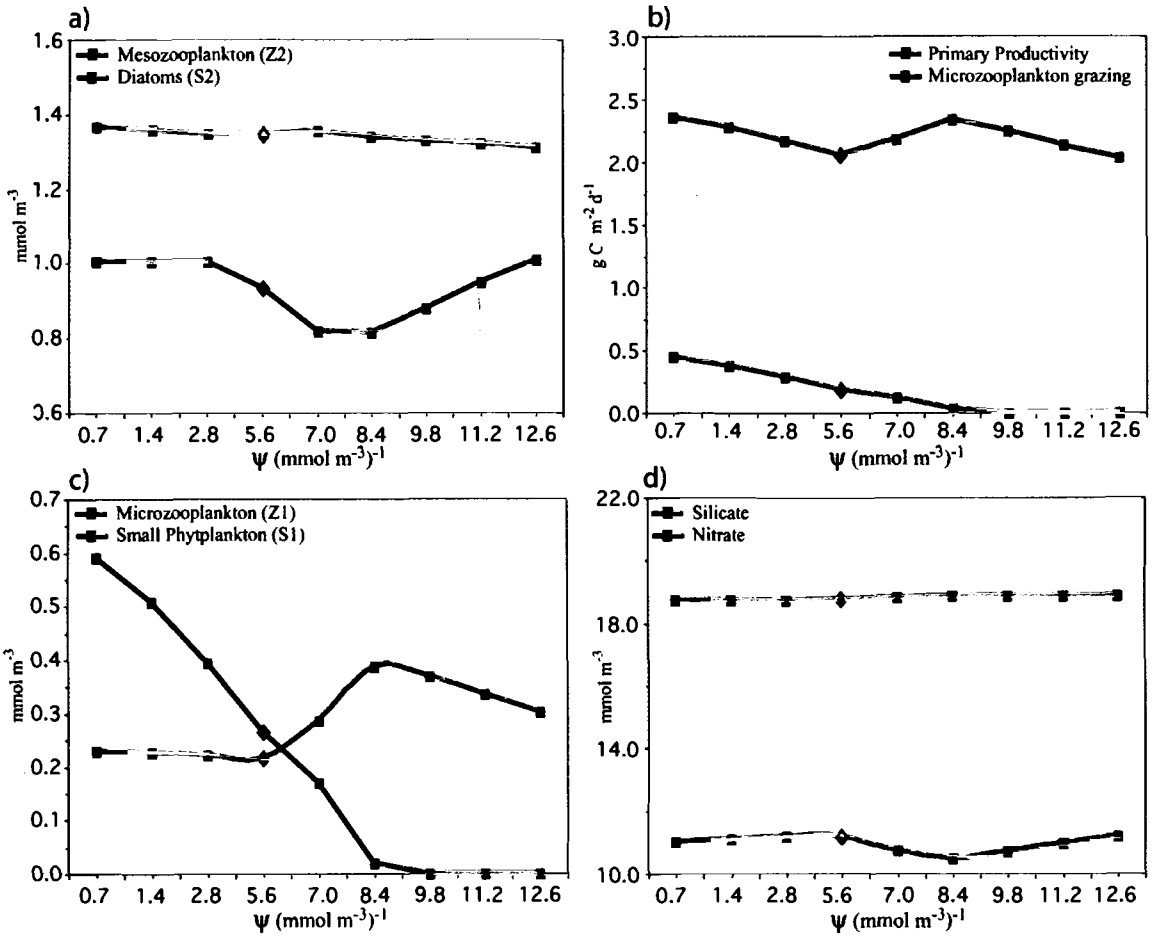

Figure 3.9: Response of several model components to changes in the parameter ψ (ammonium inhibition parameter). a) Mesozooplankton and Diatoms, b) Primary Productivity and Mesozooplankton grazing, c) Microzooplankton and Small Phytoplankton, d) Silicate and Nitrate. The control of the sensitivity study is indicated by a reverse colored diamond.

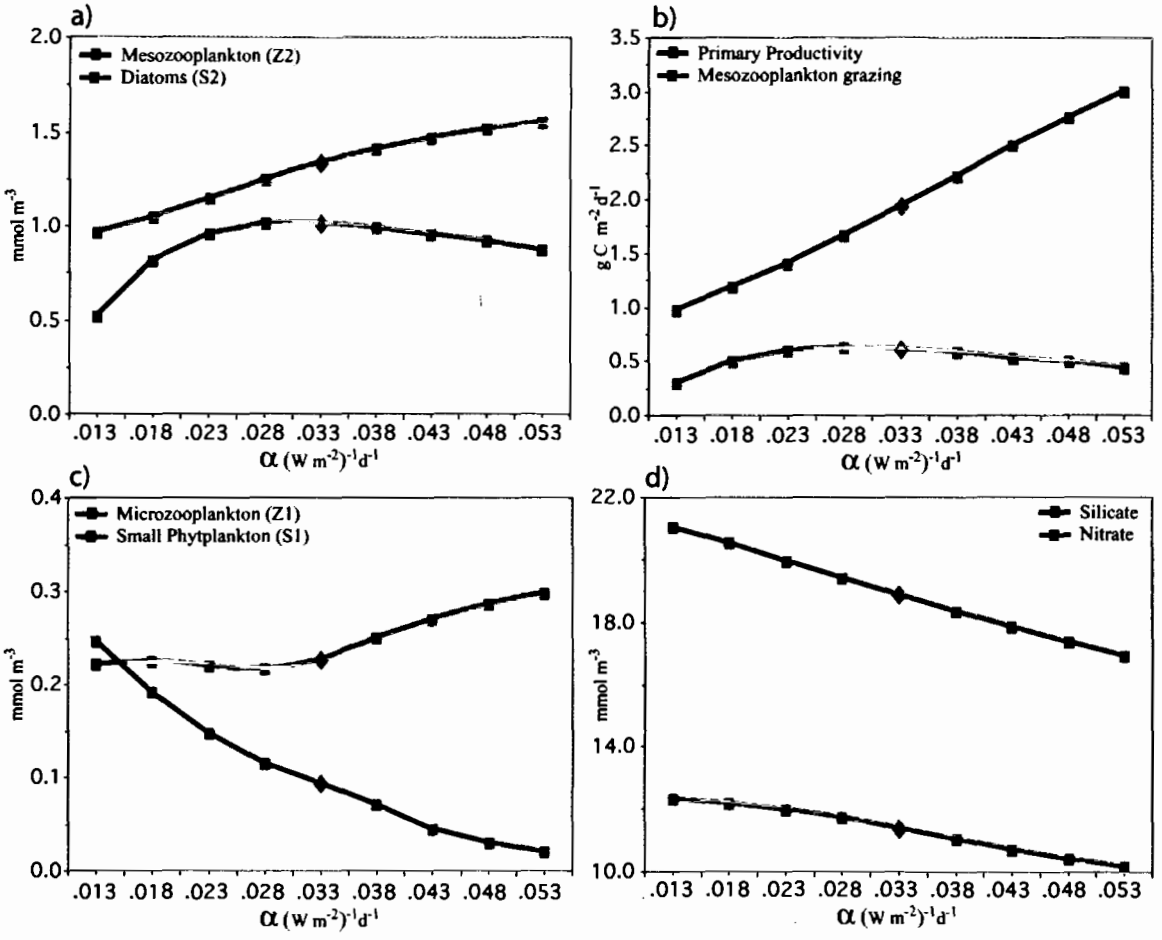

Figure 3.10: Response of several model components to changes in the parameter α (initial slope of P-I curve). a) Mesozooplankton and Diatoms, b) Primary Productivity and Mesozooplankton grazing, c) Microzooplankton and Small Phytoplankton, d) Silicate and Nitrate. The control of the sensitivity study is indicated by a reverse colored diamond.

Chapter 4

INTERANNUAL VARIABILITY

Interannual Variability in the Monterey Bay Region

After reproducing the seasonal cycle of nutrient dynamics and biological productivity in the Monterey Bay, the next step was to modify the seasonal model in order to simulate interannual variability. In order to simulate the response of biogeochemical cycle to the interannual physical variation in Monterey Bay, the seasonal forcing used in the previous study was modified from a repeating one-year loop to continuous observed data for over a decade, from 1990 to 2000. The goal of the interannual variability study was to use the model to investigate how nutrient dynamics and phytoplankton productivity respond to El Niño and La Niña events in the Monterey Bay.

El Niño Southern Oscillation (ENSO) is a coupled ocean-atmosphere phenomenon that refers to a "seesaw" movement in both surface air pressure and the oceanic thermocline across the Pacific Ocean basin. However, these events are not limited only to the equatorial Pacific. They are believed to influence the entire global climate. While the determination of a precise cause is still subject to theory, scientists do agree that coastal California has a direct "teleconnection" to the equatorial ENSO events (Chavez, 1996; Kudela and Chavez, 2000).

Some investigators attribute effects of ENSO in California to an expansion of the Aleutian Low, a low-pressure center located near the Aleutian Islands, representing one

of the main centers of activity in the atmospheric circulation of the Northern Hemisphere (Simpson, 1984). Others argue that oceanic Kelvin waves which are associated with density fluctuations inside the ocean, generated by strong westerly bursts of wind over warmer than normal Pacific ocean waters, are strongly linked to atmospheric events in the western Pacific (Chavez, 1996).

It has been noted that Kelvin waves are capable of depressing the thermocline upon reaching the South American coastline, and larger occurrences, such as El Niño 1997-1998, can be directly attributed to this phenomenon. However, studies have shown that the Kelvin waves do not stop upon reaching the eastern equatorial Pacific. The waves become coastally trapped and continue to propagate to the north and south along the American coast (Enfield and Allen 1980; Huyer and Smith, 1985; Chavez, 1996). Chavez (1996) argues that these waves directly affect temperature and salinity along the California coast, indicated by "warm, fresh water associated with downwelling and northward flow along the coast, elevated sea-surface temperatures, a deepened thermocline, and severely decreased surface nutrient concentrations in central California (Chavez, 2000)."

A useful indicator of the state of an ENSO event is derived from the Southern Oscillation Index (SOI). The index is calculated from monthly fluctuations in the air pressure difference between the island of Tahiti and Darwin, Australia. Prolonged negative values of the SOI often indicate El Niño episodes. In association with the negative values is a decrease in the strength of the equatorial trade winds, and a western suppression of the thermocline causing warm upwelling off the Pacific coast of South America. Positive SOI values are generally associated with La Niña, El Niño's extreme

opposite. The most recent strong El Niño event occurred in 1997-1998, however a weak to moderate prolonged event occurred between 1991-1995, reaching a maximum in 1992. A moderate La Niña occurred in 1999. This plethora of ENSO activity between 1990 and 2000 makes it a particularly interesting decade to study, and the model aids in understanding the linkage between the physical and biological processes in the California upwelling system.

Modification of the Forcing in the Model

In order to simulate biological responses to the interannual physical variability in the Monterey Bay, the forcing used in the model needed to be modified according to the availability of the observations. Specifically, the PAR values from M1 were derived from raw daily values from 1992-2000. A 90-day running mean was applied to the entire data set to remove high frequency background noise in order to obtain a more clear interannual signal.

PFEL's live access server (LAS) supplied the upwelling index values for the nine-component model's interannual simulations. A daily upwelling index was derived from wind values for 1990-2000. The values' units were converted from $m^3 s^{-1} 100 m^{-1}$ of coastline to $m d^{-1}$in order to coincide with the model input format and units. Similar to the treatment of the PAR data set, a 90-day running mean was applied to the upwelling index values.

Because no complete nutrient data set existed for the entire period, interannual nutrient concentrations were calculated based upon temperature-nutrient relationships,

and combined with the MBARI temperature record over an eleven-year period (1990-2000). In order to calculate the temperature below the mixed layer, a cosine function was formulated to create the thermocline strength (TS) (Olivieri and Chavez, 2000). The TS, the difference between the SST and the temperature at the bottom of the thermocline (set at 40m for Monterey Bay modeling purposes), was subtracted from SST to reflect winter vertical mixing and summer stratification for temperature below the thermocline. Based on O&C's second-order regression, nitrate values were derived from the modified SST (Figure 4.1). This nitrate-temperature relationship was based upon samples collected from moorings M1 and H3 between 10 and 60 meters from 1989-1995. Mooring H3, the precursor to mooring M1, is located only 3 km north of mooring M1. The data from the two moorings are often combined into one continuous set. A third-order regression was formulated in order to derive $Si(OH)_4$ from NO_3 (Figure 4.1).

Observed values of upwelling velocity, SST, and regressed NO_3 were graphed over the eleven-year period in order to determine whether they shared common interannual signals, as well as to have a record to which modeled results could be compared (Figure 4.2). Temperature and nitrate (silicate was very similar to nitrate) depicted the 1997-1998 El Niño very well with higher temperature and lower nitrate concentration. The interannual signals that nitrate depicted confirmed that the regressions used to derive the nutrient concentrations were successful (Figure 4.2c). Temperature values increased over the period as warm water was upwelled, replacing the usual cold, nutrient rich waters. NO_3 also followed the El Niño pattern with a distinct depression during the 1997-1998 El Niño event, representing the low nutrient, warm water, associated with El Niño (Figure 4.2b, c).

Both nitrate and temperature variations during the period, along with upwelling velocities (Figure 4.2a), clearly depict the transition of El Niño 1997-1998 into the moderate La Niña of 1999-2000. The observed upwelling velocities agreed with daily mean upwelling velocities from a 12-year data set of upwelling indices calculated for Monterey Bay (Mason and Bakun, 1986). The calculated results ranged from -1.5 m d^{-1} (downwelling) to 5.6 m d^{-1} (upwelling) (Olivieri and Chavez, 2000). The inverse-relationship of temperature and nutrient concentrations is represented in Figure 4.2a and b, illustrating a significant temperature decrease and nutrient increase as La Niña conditions make for favorable deep, cold, and nutrient rich waters to upwell to the surface. Figure 4.2a further supports this behavior, depicting a large peak, corresponding to stronger upwelling, in 1999.

SST Anomaly, SOI, Nutrient Flux, and PAR

Another method of recording the duration and intensity of ENSO events is by analyzing the sea surface temperature anomalies in the equatorial Pacific. Opposite of the SOI values, positive anomalies represent El Niño events, while negative ones are indicative of La Niña episodes. Long period and large amplitude episodes indicate particularly intense events, such as the El Niño of 1997-1998 (Figure 4.3). One is also able to discern the weak to moderate but prolonged 1991-1995 El Niño (positive, red) signal, as well as the weak La Niña of 1999 (negative, blue).

Returning to observed SOI values, the SOI index correlated very well with the SST anomaly (Figure 4.4a). As described earlier, negative values correlate to an El Niño

event, while positive values indicate a La Niña episode. Again, it was very easy to distinguish the similar patterns that represent the 1991-1995 and 1997-1998 El Niños and the 1999 La Niña. For comparison, nutrient flux anomaly (departure from the mean seasonal values of $(NO_3 + Si(OH)_4)$* Upwelling) and PAR anomaly are also depicted in the same figure (Figure 4.4b, c). It is worth noting that nutrient flux values are positive during La Niña events and negative during El Niños. This is derived from the fact that La Niña events in California are characterized by deep, nutrient rich, coastal upwelling while El Niño events, as mentioned earlier, are distinguished by decreasing nutrient flux due to diminished upwelling velocities and lower nutrient concentrations in the subsurface waters. An interesting observation of the nutrient flux anomaly was that it detected the 1999 La Niña signal almost three times as strongly as both the 1991-1995 and 1997-1998 El Niños. This occurrence is most likely attributable to a combination of much higher than normal nutrient concentrations and higher than typical upwelling velocities during the La Niña episode.

PAR anomaly maintained an interesting interannual variation (Figure 4.4c). The 1997-1998 signal depicted a strong positive anomaly in the beginning of the event. However, the anomaly precipitously dropped to zero in the beginning of 1998, possibly attributed to the seasonality of the event. The anomaly also detected the La Niña signal of 1999 with strong negative values associated with much lower than normal light levels. PAR values can be quite variable merely due to local weather patterns. However, on a much larger, more seasonal scale, ENSO effects influenced Monterey Bay light levels as well.

Typically Monterey Bay water temperatures are much cooler than the coastal air temperature, especially during strong upwelling events associated with La Niña. The temperature difference between the water and air masses result in the formation of fog and low lying clouds. The fog and cloud cover, absorb and reflect much of the solar radiation that would typically reach the ocean surface. Hence, PAR levels were abnormally low during the La Niña event (Figure 4.5c). The opposite applies to the El Niño events. Because the ocean temperature is warmer due to the lack of upwelling, the air-sea temperature difference is reduced during the El Niño events, and hence the atmosphere remains relatively clear. This resulted in higher than normal light levels, or positive PAR anomalies during the El Niño periods (Figure 4.5c).

Modeled Nitrate Concentration and Small Phytoplankton

The modeled NO_3 concentration for the eleven-year duration is shown in Figure 4.5a. The modeled results compare very well with the observed NO_3 data (Figure 4.2c). The other two panels represent modeled small phytoplankton (S1) and modeled small phytoplankton anomaly (mean seasonal cycle removed) (Figure 4.5b, c). Modeled NO_3 capably detected both the 1991-1995 (1992) and the 1997-1998 El Niños, as well as the 1999 La Niña. As previously mentioned, the El Niño signal is associated with lower than normal nutrient values, while the La Niña signal is quite the opposite. While both the S1 and the S1 anomaly show insignificant changes during the weaker 1992 El Niño, both detected the lower than normal conditions in 1997. Indicative of an El Niño event, the low nutrient levels represented the cessation of upwelling. With a lack of upwelling,

there is no mechanism to deliver nutrient rich, deep water to replace the nutrient exhausted surface waters. With a slight time delay, as the remaining nutrients are depleted, S1 and S1 anomaly precipitously dropped off, following the nutrient concentration changes. As the NO_3 level began to recover in the following year, S1, tightly fitted to nutrient responses, also began to recover very rapidly. This explains why the S1 response, for both total concentration and the anomaly, gave the impression of leading the nitrate concentration (Figure 4.5). As it moved into La Niña in 1999, the nitrate concentration continued to increase. However, the S1 biomass had already reached its maximum earlier in the season. This can be attributed to an irregular supersaturation of available nitrate that leads to self-shading (when a population is so dense that the upper phytoplankton prevent the light from reaching the phytoplankton lower in the water column), flocculation (organisms and particles form conglomerates that more rapidly sink out of the water column), as well as grazing by zooplankton. All of these factors could lead to an earlier peak followed by a decline in the small phytoplankton population.

Modeled Silicate Concentration and Diatoms

The modeled silicon cycle was divided in much the same fashion as the nitrogen cycle (Figure 4.6). Modeled $Si(OH)_4$ depicted the El Niños and La Niña just as effectively. However, modeled diatoms (S2) and modeled S2 anomaly while capable of detecting both El Niños quite well, showed a lack of response during the 1999 La Niña.

The S2 anomaly is important to depict because it clearly showed the depression in the S2 population as a result of the decrease in $Si(OH)_4$ concentration.

While it is uncertain why S2 did not depict the La Niña signal, it is important to remember that the S2 population is not only affected by $Si(OH)_4$, but also NO_3 and NH_4. The inability for modeled silicate to detect the La Niña could be due to the fact that the diatom population could already be saturated with $Si(OH)_4$ so any additional influx of nutrients would show no effects on the diatom biomass. Other Monterey Bay studies have shown that while silicate can sometimes be the regulating nutrient, it is actually nitrate that plays a dominant role during El Niño events (Kudula and Chavez, 2000; Kudula and Dugdale, 2000). These results hint at the possibility that even during periods of low nutrient flux, there still might be enough silicate to allow for diatom growth.

Primary Production

The PP was also calculated for interannual variability (Figure 4.7). While the seasonal signal of PP increased during the upwelling season, the only interannual signal that could be detected with any significance was the 1992 El Niño. As expected, this signal was represented by a depression in the PP, resulting from low nutrient values during that period. The modeled PP curve fit the observed biweekly PP values quite well (Figure 4.7). While it remains somewhat unclear why the strong ENSO signals from 1997-1998 or 1999 didn't appear in either the modeled or the observed PP, it is obviously linked to earlier discussions on the responses of S1 and S2 to the fluctuating nutrient levels as well as light intensity changes during the ENSO events.

A study conducted by Kudula and Chavez (2000) showed a slight depression in primary productivity at the beginning of the 1992 El Niño season. However, as the season progressed, little difference between the annual rates for 1992 and non-ENSO records was observed. Results, similar to the nine-component model diatom results, indicated that chlorophyll levels were also found to be somewhat resistant to the effects of El Niño. The hypothesis presented in Kudula and Chavez's (2000) study for why PP and Chl were relatively unaffected was that even with the reduced nutrient supply to Monterey Bay, there was still enough to maintain normal levels of biological productivity. However, further offshore, away from the upwelling zones, it was proposed that productivity levels would plummet drastically. Hence, normal productivity levels would only be maintained at the source of upwelling, and productivity would be dramatically reduced further away from the upwelling origins. While there have been very few papers published on the effects of the 1997-1998 El Niño, one could potentially assume that similar mechanisms, as proposed by Kudula and Chavez (2000), were at work during this period, as well. This thesis work provides the first modeled evidence on how nutrients, biological productivity, and chlorophyll responded to the 1997-98 ENSO event in the Monterey Bay.

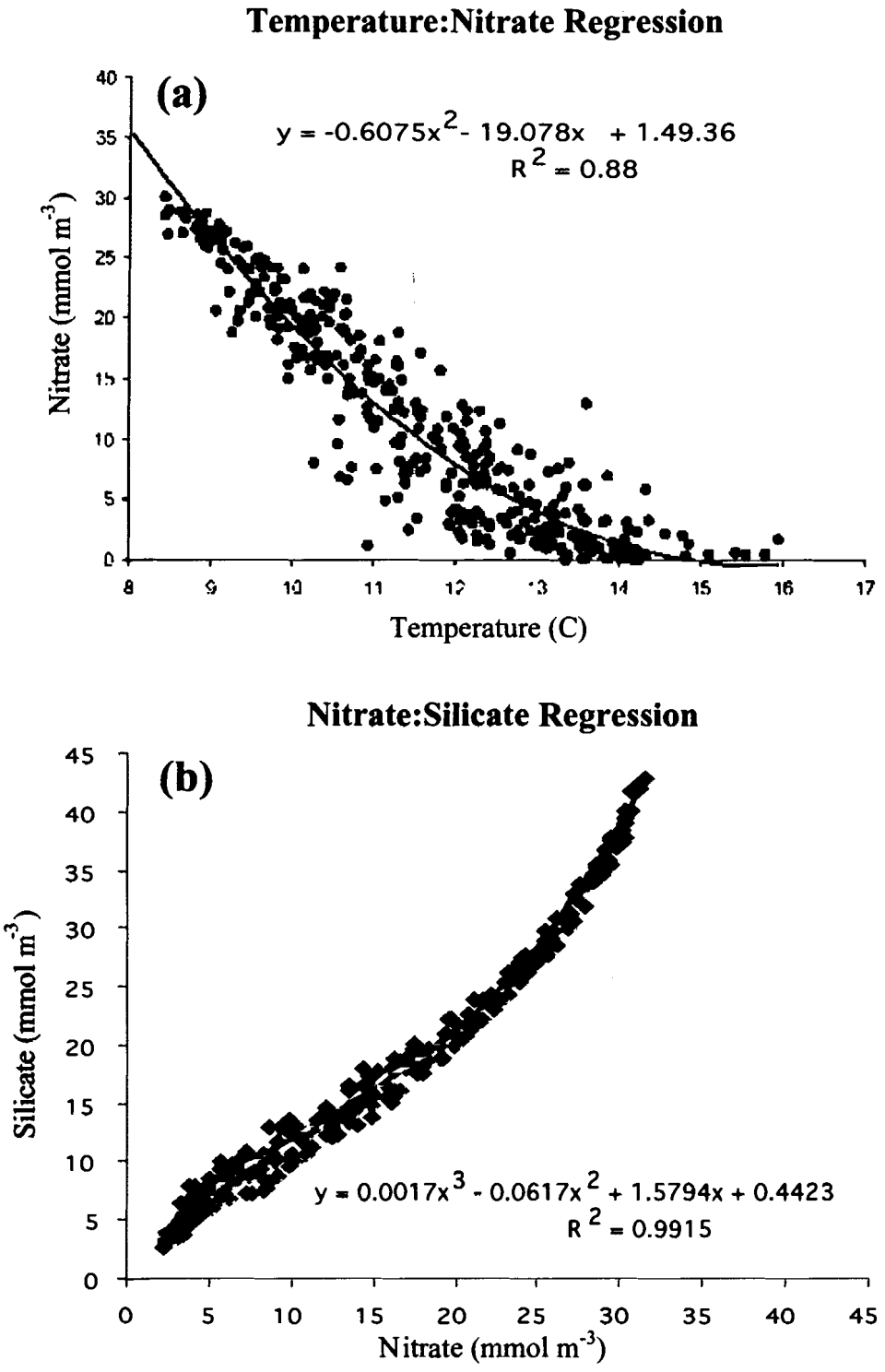

Figure 4.1: Regression curves. (a) Second-order regression of nitrate versus temperature. Samples collected at stations H3 and M1 mooring from 1989 to 1995 from depths 10-60 m (modified from Olivieri and Chavez, 2000). (b) Third-order regression of silicate versus nitrate. Samples collected at station M1 mooring from 1989 to 2000 from depths 0-200 m.

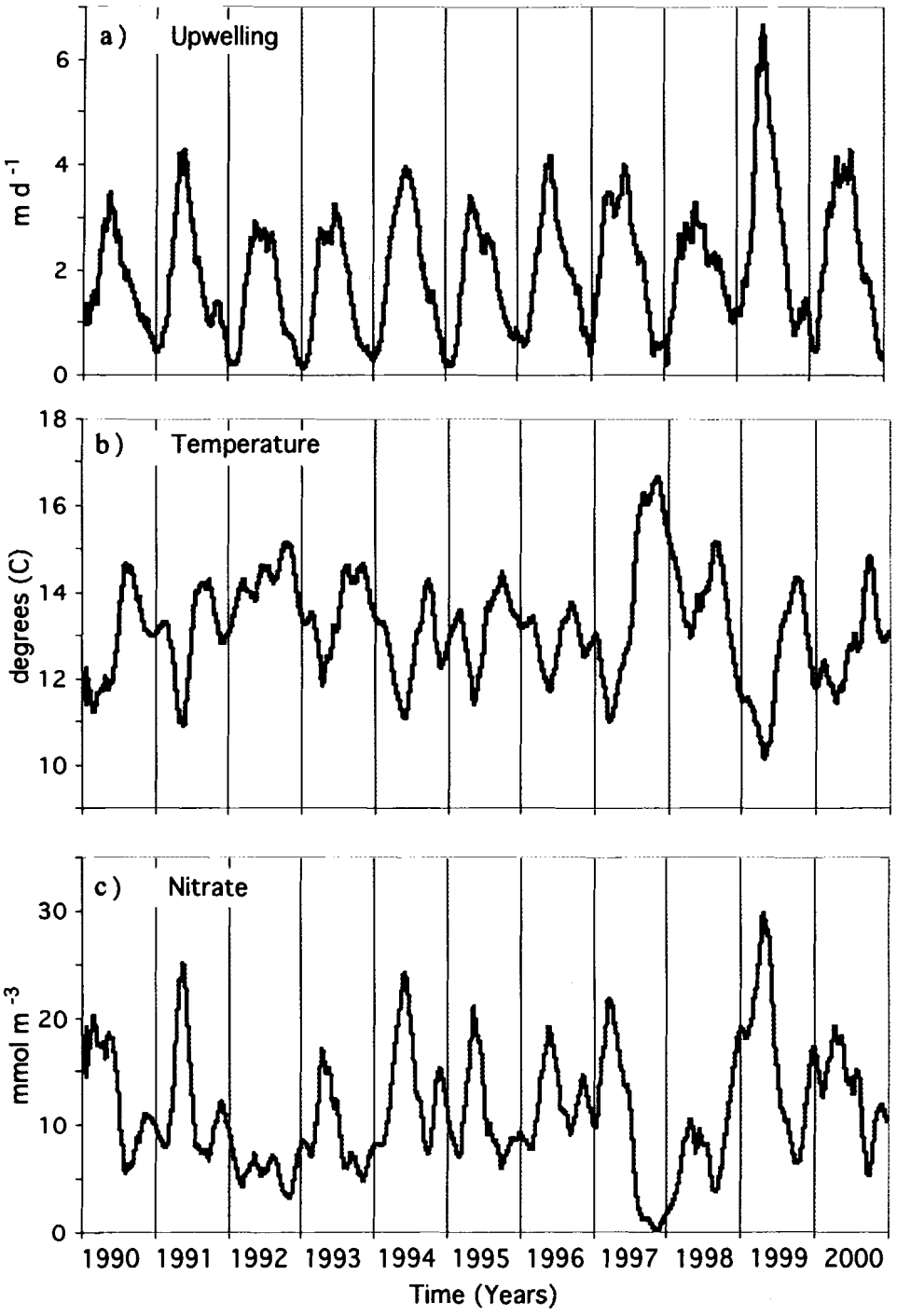

Figure 4.2: Observed values of three Monterey Bay parameters. a) Observed upwelling values. b) Observed temperature values. c) Temperature regressed nitrate values. The interannual silicate signal closely matched that of nitrate.

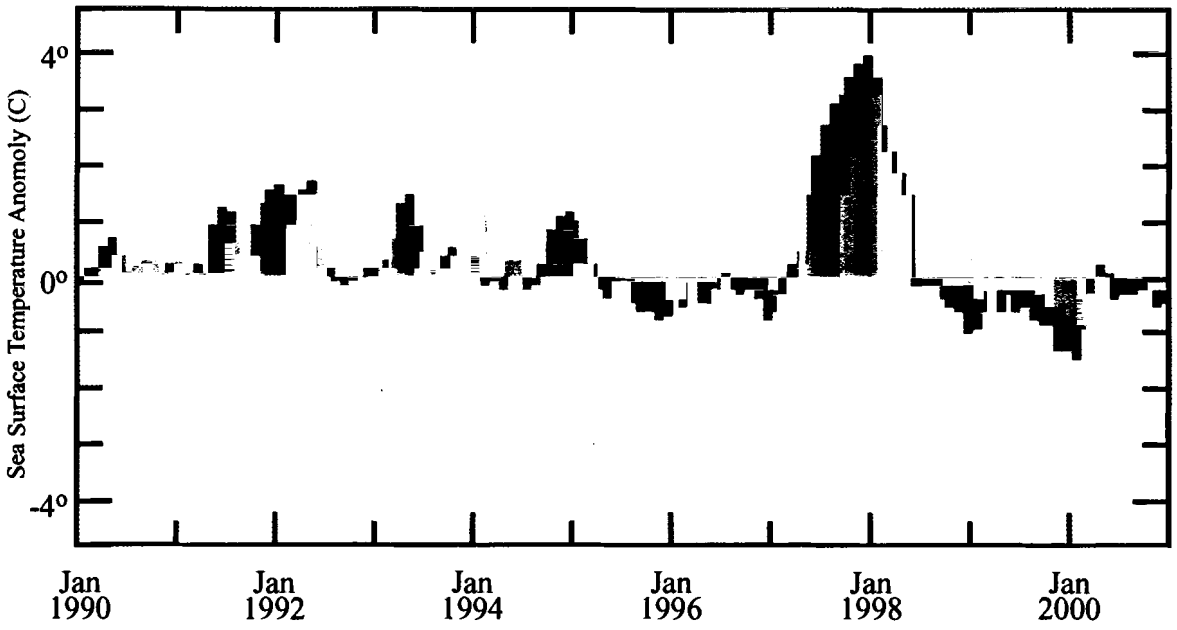

(modified from http://ingrid.ldgo.columbia.edu/SOURCES/.Indices/ensomonitor.html)

Figure 4.3: Sea surface temperature anomaly (from the eastern equatorial Pacific) is an index that is an indicator of the strength of an ENSO event. Sustained positive values (reds) indicate an El Niño event while negative values (blues) indicate a La Niña occurrence.

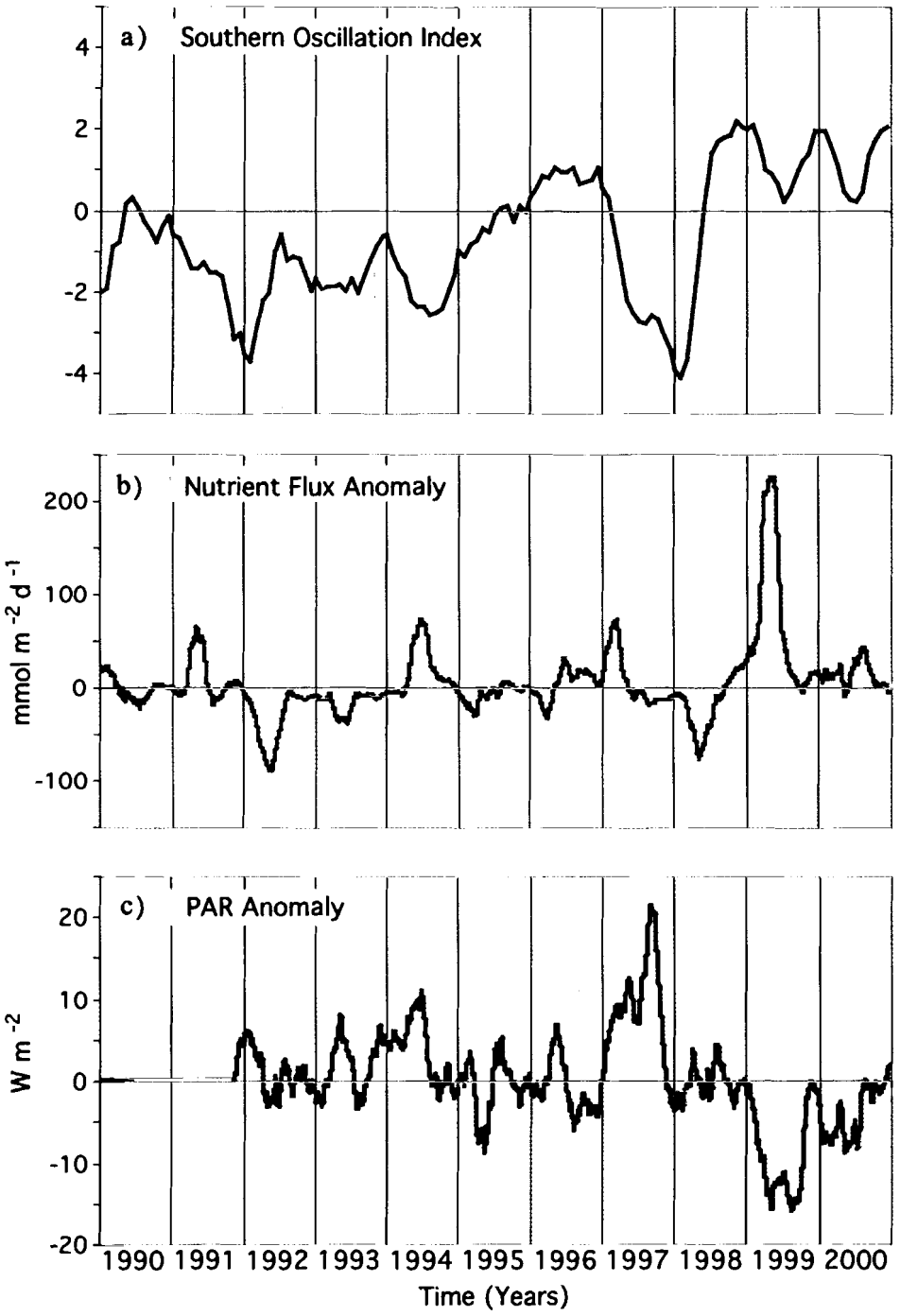

Figure 4.4: Three El Niño Southern Oscillation (ENSO) indicator parameters. a) Calculated Southern Oscillation Index (SOI) b) Observed nutrient flux anomaly. c) Observed PAR anomaly (No PAR data 90-91).

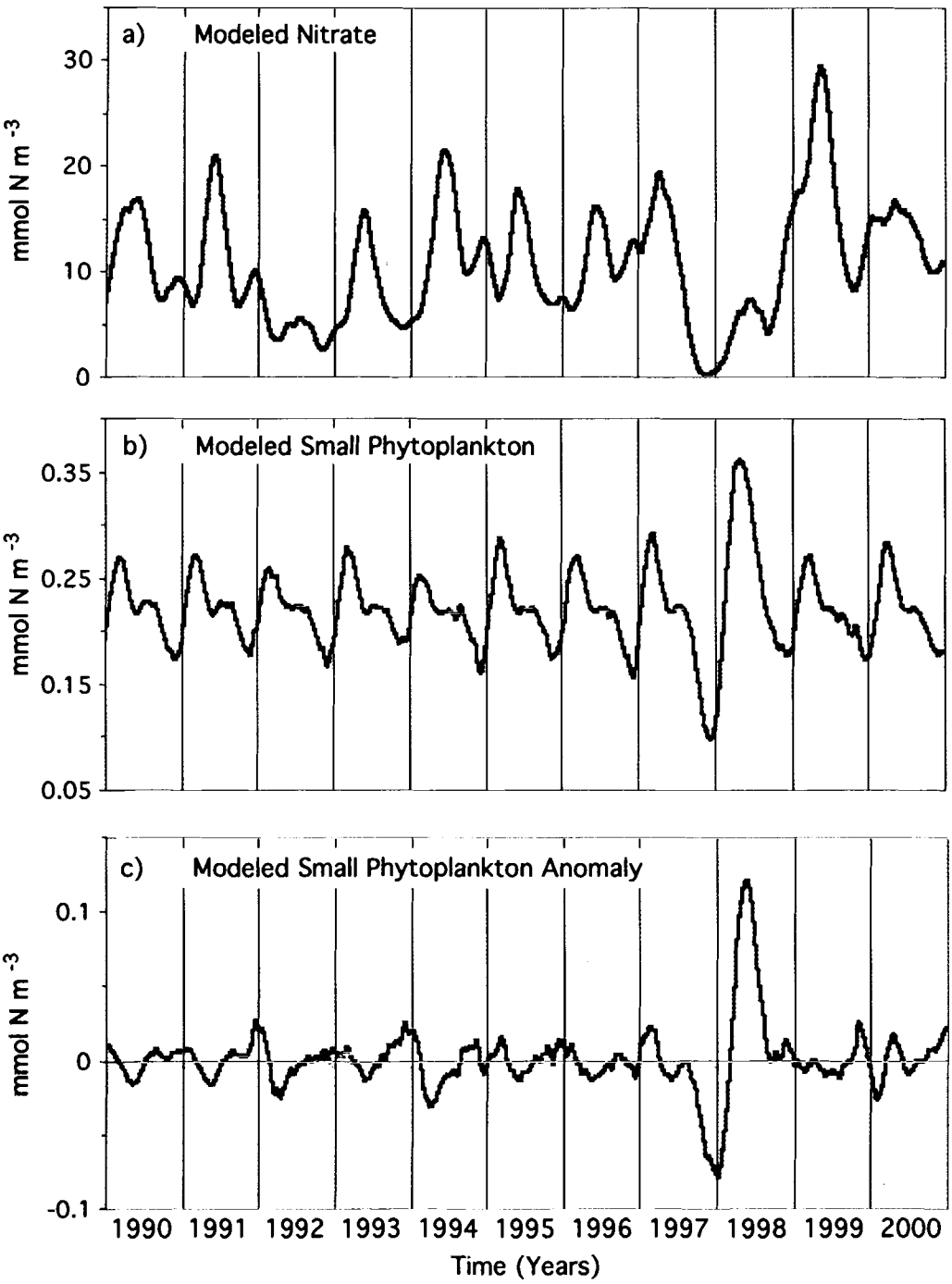

Figure 4.5: Three nine-component interannual model nitrate cycle values. a) Interannual nitrate values estimated by the nine-component model. b) Interannual small phytoplankton (S1) values estimated by the nine-component model. c) Interannual small phytoplankton anomaly values estimated by the nine-component model.

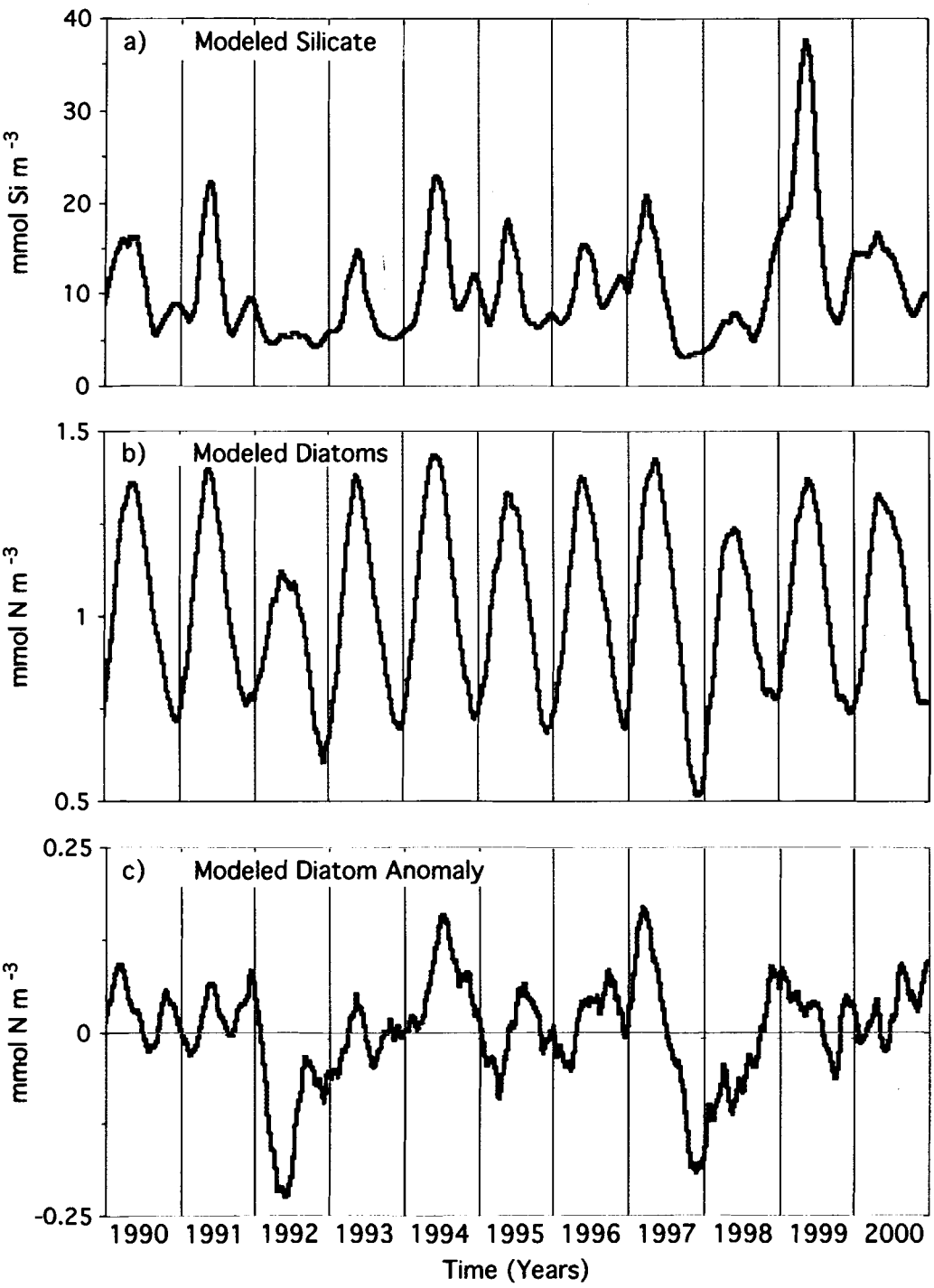

Figure 4.6: Three nine-component interannual model silicate cycle values. a) Interannual silicate values estimated by the nine-component model. b) Interannual diatom (S2) values estimated by the nine-component model. c) Interannual diatom anomaly values estimated by the nine-component model.

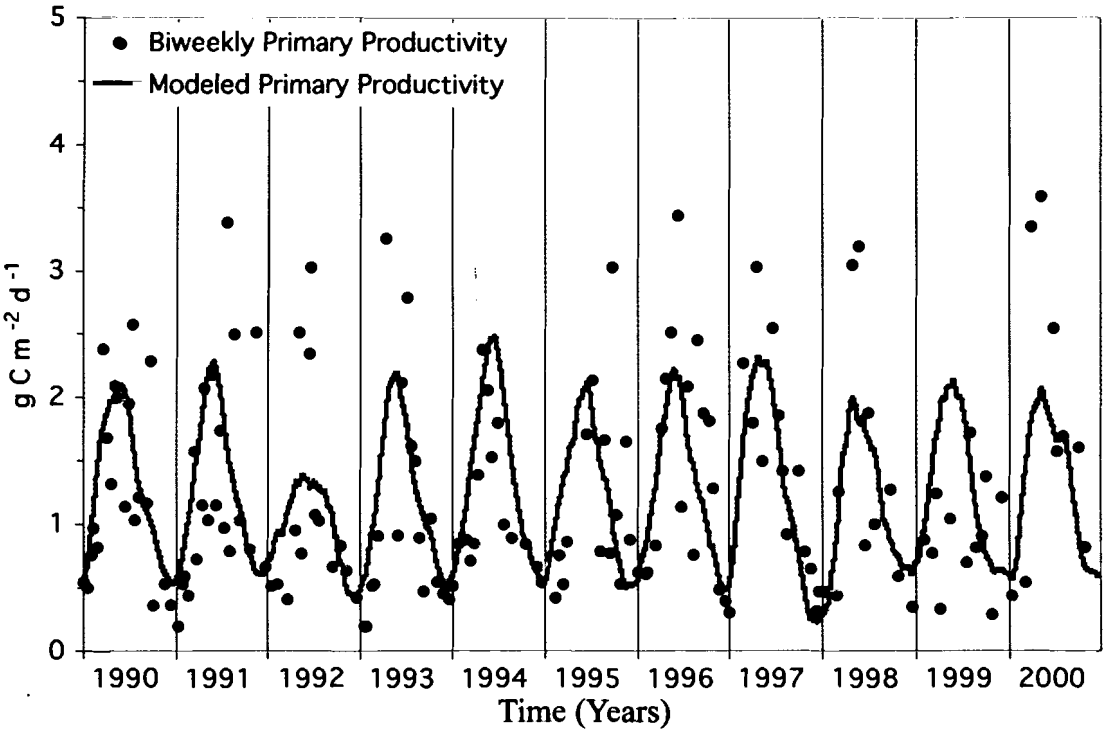

Figure 4.7: Interannual cycle of primary productivity. Modeled values versus biweekly observed values.

Chapter 5

CONCLUSIONS

A nine-component ecosystem model was developed for the Monterey Bay upwelling system. The model was adapted and modified from the previous endeavors of Olivieri and Chavez (2000) and Chai et al (2002), to address the seasonal cycle and interannual variability of nutrient dynamics and phytoplankton productivity in the Monterey Bay, California. The nine-component model was forced with observed nutrients, upwelling velocity, and surface light values. It was capable of reproducing seasonal and interannual variations of nutrient concentrations, phytoplankton and zooplankton biomass, as well as primary productivity and grazing rates.

The seasonal cycle modeling effort was highly successful in creating a general model to reproduce nutrients, chlorophyll, and primary productivity with great accuracy compared to the long-term climatological data at the M1 mooring. By using annual mean upwelling velocity and surface light, and comparing results with the "control run" (with full seasonal cycle in these forcing), the model results showed that the upwelling velocity determines overall nutrient concentrations, while solar radiation controls primary productivity and chlorophyll levels. The modeled f-ratio for the seasonal cycle study was also quite reasonable, depicting high f-ratio values during the spring and summer upwelling seasons, and low values during the winter months when regenerated production dominates.

A series of model sensitivity studies has been conducted by varying one parameter at a time. The results of the sensitivity studies are as follows:

1. The effects of both meso- and microzooplankton grazing were tested by varying $G2_{max}$ and $G1_{max}$, meso- and microzooplankton grazing rates, in two respective studies. The modeled results showed that both parameters are very sensitive in controlling the total phytoplankton and zooplankton biomass, as well as the production and grazing rates. However, the nutrient concentrations are not sensitive to these two grazing parameters. One theory that explains the insensitivity is that the Monterey Bay upwelling system is saturated with excess nutrients due to the high upwelling supply of nutrient-rich water.
2. The ammonium inhibition parameter, ψ, is an important factor in determining the nitrogen cycle in the nine-component model. It greatly affects primary productivity, which is the sum of new and regenerated production, as well as microzooplankton population due to the overall reduction of small phytoplankton.
3. Two parameters responsible for controlling diatom population, α (initial slope of P-I curve) and $K_{Si(OH)4}$ (half-saturation for silicate uptake), were both individually modified in order to test diatom population response to these two parameters. Increasing α resulted in a linear increase in the diatom population, a linear decrease in nutrients, and an overall increase in primary production. Increasing $K_{Si(OH)4}$, however, had the opposite effects by decreasing the diatom population, increasing nutrients, and overall decreasing the primary productivity of the system .

Once the seasonal model was refined and understood, eleven years of observed physical forcing data was used to drive the nine-component ecosystem model in order to address the ecosystem responses to interannual climate variability. The model was capable of reproducing lower nutrient concentrations and reductions in phytoplankton biomass and productivity during two El Niño events during the 1990s. The two events were the long duration 1991-95 warm period (with 1992 being the maximum) El Niño, and a strong 1997-98 El Niño. The model also responded to a moderate 1999 La Niña event with higher nutrients, enhanced productivity, and elevated phytoplankton biomass, especially in the modeled diatoms. The modeled results compared favorably with the time series observations in the Monterey Bay.

The success of this modeling endeavor was due greatly to the fact that MBARI had the insight to establish the time series observations, a wealth of data, almost two decades ago. This impressive collection has sparked much interest and research activities in studying upwelling dynamics, not only in the Monterey Bay, but also for other upwelling systems throughout the world oceans.

The nine-component ecosystem model was developed by using the Systems Thinking in an Experimental Learning Lab with Animation (STELLA), which is a hands-on, non-language-programming modeling package. The benefits of using such a modeling package include reduced modeling time, more user-friendly design template, and most importantly, the introduction of modeling to non-programming scientists and the general public.

Future work could expand the STELLA nine-component model to include more components, such as carbon cycle to address air-sea carbon dioxide exchange, thereby increasing its complexity. Another enhancement to the nine-component model could include adding a depth dimension in order to allow the euphotic-zone-depth to vary with time. Lastly, it would be interesting to apply this nine-component ecosystem model to other upwelling regions, such as coastal Peru or the Georges Bank located in the Gulf of Maine, in order to test the limitations of this model. Throughout comparison studies between different upwelling systems, scientists can continue to improve upon ecosystem models in order to gain further understanding of how marine ecosystems may respond to future climate change and other pressing global issues.

BIBLIOGRAPHY

Abbott, M.R., Zion, P.M., 1985. Satellite observations of phytoplankton variability during an upwelling event. Continental Shelf Research 4, 661-680.

Barber, R.T., Smith, R.L., 1981a. Coastal upwelling ecosystems. In: Longhurst, A.R. (Ed.), Analysis of Marine Ecosystems. Academic Press, New York, pp. 31-68.

Barber, R.T., Smith Jr., W.O., 1981b. The role of circulation, sinking, and vertical migration in physical sorting of phytoplankton in the upwelling center at 153S. In: Richards, F.A. (Ed.), Coastal Upwelling. American Geophysical Union, Washington DC, pp. 366-371.

Barber, R.T., Chavez, F.P., 1991. Regulations of primary productivity rate in the equatorial Pacific. Limnology and Oceanography 36 (8), 1803-1815.

Bidigare, R. R., Ondrusek, M. E., 1996. Spatial and temporal variability of phytoplankton pigment distributions in the central equatorial Pacific Ocean. Deep-Sea Research II 43, 809-833.

Brink, K.H., 1983. The near-surface dynamics of coastal upwelling. Progress in Oceanography 12, 223-257.

Brink, H.K., Abrantes, F.F.G., Bernal, P.A., Dugdale, R.C., Estrada, M., Hutchings, L., Jahnke, R.A., Muller, P.J., Smith, R.L., 1995. Group report: how do coastal upwelling systems operate as integrated physical, chemical, and biological systems and influence the geological record? The role of physical processes in defining the spatial structures of biological and chemical variables. In: Summerhayes, C.P., Emeis, K.-C., Angel, M.V., Smith, R.L., Zeitzschel, B. (Eds.), Upwelling in the Ocean: Modern Processes and Ancient Records. Wiley, New York, pp. 103-124.

Brzezinski, M.A., 1985. The Si:C:N ratio of marine diatoms. Interspecific variability and the effect of some environmental variables. J. Phycol. 21, 347-357.

Brzezinski, M., Phillips, D., Chavez, F., Friedrich, G., Dugdale, R., 1997. Silica production in the Monterey, California upwelling system. Limnol. Oceanogr. 42(8), 1694-1705.

Bureau of Meteorology, Commonwealth of Australia 2002, SOI download http://www.bom.gov.au/climate/current/soihtm1.shtml

Chai, F., 1996. Origin and maintenance of a high NO_3 condition in the equatorial pacific, a biological-physical model study. The school of the environment, Duke University. PhD dissertation, 1995.

Chai, F., Lindley, S.T., Barber, R.T., 1996. Origin and maintenance of a high NO_3 condition in the equatorial pacific. Deep Sea Research II 43, 1031-1060.

Chai, F., Lindley, S.T., Toggweiler, J. R., Barber, R.T., 1999. Testing the importance of iron and grazing in the maintenance of the high nitrate condition in the Equatorial Pacific Ocean, a physical-biological model study. In: Hanson, H.W. Ducklow, & J.G. Field (Editors), 1999. The Changing Ocean Carbon Cycle. International Geosphere-Biosphere Programme (IGBP) Book Series 5. Cambridge University Press, pp. 156-186.

Chai, F., Dugdale, R.C., Peng, T-H, Wilkerson, F.P., Barber, R.T., 2002. One dimensional ecosystem model of the equatorial Pacific upwelling system, part I: Model development and silicon and nitrogen cycle. Final version for Deep Sea Research II.

Chavez, F.P., Barber, R.T., 1987. An estimate of new production in the equatorial Pacific. Deep-Sea Research 34, 1229-1243.

Chavez, F.P., Barber, R.T., Huyer, A., Kosro, P.M., Ramp, S.R., Stanton, T., Rojas de Mendiola, B., 1991. Horizontal advection and the distribution of nutrients in the coastal transition zone of northern California: effects on primary production, phytoplankton biomass and species composition. Journal of Geophysical Research 96, 14833, 14848.

Chavez, F.P., 1996. Forcing and biological impact of onset of the 1992 El Niño in central California. Geophysical Research Letters 23, 265-268.

Chavez, F.P., Pennington, J.T., Herlien, R., Jannasch, H., Thurmond, G., Friederich, G.E., 1997. Moorings and drifters for real-time interdisciplinary oceanography. Journal of Atmospheric and Oceanic Technology 14, 1199-1211.

Chelton, D.B., Bernal, P.A., McGowan, J.A., 1982. Large-scale interannual physical and biological interaction in the California Current. Journal of Marine Research 40, 1095-1125.

Cuhel, R.L., Ortner, P.B., Lean, D.R.S., 1984. Night synthesis of protein by algae. Limnology and Oceanography 29(4), 731-744.

Dagg, M., Cowles, T., Whitledge, T., Smith, S., Howe S., Judkins, D., 1980. Grazing and excretion by zooplankton in the Peru upwelling system during April 1977. Deep-Sea Research, 27A.

Dortch, Q., 1990. The interaction between ammonium and nitrate uptake in phytoplankton. Marine Ecology Progress Series 61, 138-201.

Dugdale, R.C., Goering, J.J., 1967. Uptake of new and regenerated forms of nitrogen in primary production. Limnology and Oceanography 12, 196-206.

Dugdale, R.C., Wilkerson, F.P., 1998. Silicate regulation of new production in the equatorial Pacific upwelling, Nature, 391, 270-273.

Enfield, D.B., Allen, J.S., 1980. On the structure and dynamics of monthly mean sea level anomalies along the Pacific coast of North and South America, Journal Geophysical Research 10, 557-578.

Eppley, R. W., Rogers, J. N., McCarthy, J. J., 1969. Half-saturation constants for uptake of nitrate and ammonium by marine phytoplankton. Limnology and Oceanography 14, 912-920.

Eppley, R.W., Peterson, B.J., 1979. Particulate organic matter flux and planktonic new production in the deep ocean. Nature 282, 677-680.

Eppley, R.W., Chavez, F.P., Barber, R.T., 1992. Standing stocks of particulate carbon and nitrogen in the Equatorial Pacific. Journal Geophysical Research 97, 655-661.

Evans, G. T., Parslow, J. S., 1985. A model of annual plankton cycles. Biological Oceanography 24, 483-494.

Fasham, M. J. R., Ducklow, H. W., McKelvie, S. M., 1990. A nitrogen-based model of plankton dynamics in the oceanic mixed layer. Journal Marine Research 48, 591-639.

Fasham, M. J. R., 1995. Variations in the seasonal cycle of biological production in subartic oceans: A model sensitivity analysis. Deep Sea Research 42, 1111-1149.

Frost, B.W., Franzen, N.C., 1992. Grazing and iron limitation in the phytoplankton stock and nutrient concentration: a chemostat analogue of the Pacific equatorial upwelling zone. Marine Ecology Progress Series 83, 291-303.

Geider, R.J., MacIntyre, H.L., Kana, T.M., 1997. Dynamic model of phytoplankton growth and acclimation: responses of the balanced growth rate and the chlorophyll a: carbon ratio to light, nutrient-limitation and temperature. Marine Ecology Progress Series, 148, 187-200.

Hoffmann, E. E., Ambler, J. W., 1988. Plankton dynamics on the outer southeastern US continental shelf Part II: a time-dependent model. Journal Marine Research 9, 235-248.

Hutchings, L., Pitcher, G.C., Probyn, T.A., Bailey, G.W., 1995. The chemical and biological consequence of coastal upwelling. In: Summerhayes, C.P., Emeis, K.C., Angel, M.V., Smith, R.L., Zeitzschel, B. (Eds.), Upwelling in the Oceans: Modern Processes and Ancient Records. Wiley, Chichester, 65-81.

Huyer, A., 1983. Coastal upwelling in the California Current system. Progress in Oceanography 12, 259-284.

Huyer, A., Smith, R.L., 1985. The signature of El Niño off Oregon, 1982-1983, Journal of Geophysical Research 90, 7133-7142.

Jamart, B. M., Winter, D. F., Banse, K., Anderson, G. C., Lam, R. K., 1977. A theoretical study of phytoplankton growth and nutrient distribution in the Pacific Ocean of the northwestern US coast. Deep Sea Research 24, 753-773.

Kelly, K.A., 1985. The influence of winds and topography on the sea surface temperature patterns over the northern California slope. Journal of Geophysical Research 90, 11783-11798.

Kudela, R.M., Chavez, F.P., 2000. Modeling the impact of the 1992 El Niño on new production in Monterey Bay, California. Deep-Sea Research II 47, 1055-1076.

Kudela, R.M., Dugdale, R., 2000. Nutrient regulation of phytoplankton productivity in Monterey Bay, California. Deep-Sea Research II 47, 1023-1053.

Landry, M. R., Barber, R. T., Bidigare, R. R., Chai, F., Coale, K. H., Dam, H. G., Lewis, M. R., Lindley, S. T., McCarthy, J. J., Roman, M. R., Stoecker, D. K., Verity, P. G., White, J. R., 1997. Iron and grazing constraints on primary production in the central equatorial Pacific: An EqPac synthesis. Limnology and Oceanography 42, 405-418.

Leynaert, A., Treguer, P., Lancelot, C., Rodier, M., 2001. Silicon limitation of biogenic silica production in the Equatorial Pacific. Deep Sea Research 48, 639-660.

Lindley, S. T., Bidigare, R. R., Barber, R. T., 1995. Phytoplankton photosynthesis parameters along 140W in the equatorial Pacific. Deep Sea Research II 42, 441-464.

McGowan, J.A., Chelton, D.B., Conversi, A., 1996. Plankton patterns, climate, and change in the California Current. California Cooperative Oceanic Fisheries Investigations Reports 37, 45-68.

Mason, J.E., Bakun, A., 1986. Upwelling index update, US West Coast, 33N-48N latitude. US Dept. of Commerce, NOAA Technical Memorandum. NMFS SWFC 67, 81.

Monterey Bay Aquarium Research Institute. "SST, Nutrients, PAR, Upwelling Indices, derived from M1 mooring and biweekly cruises, 1989-2000." [Computer files and websites http://www.mbari.org/bog/NOPP/data.htm, http://www.mbari.org/oasis/data_archive.html]. Moss Landing, California.

Murray, J. M., Barber, R. T., Bacon, M. P., Roman, M. R., Feely, R. A., 1994. Physical and biological controls on carbon cycling in the equatorial Pacific. Science 266, 58-65.

NOAA, Office of Global Programs, ENSO http://www.ogp.noaa.gov/enso/

Noble, M.A., Ramp, S.R., 2000. Subtidal currents over the central California slope: evidence for offshore veering of the undercurrent and for direct, wind-driven slope currents. Deep Sea Research Part II, Topical Studies in Oceanography 47 (5-6), pp. 871-906.

Olivieri, R.A., Chavez, F.P., 2000. A model of plankton dynamics for the coastal upwelling system of Monterey Bay, California. Deep Sea Research II 47, 1077-1106.

Pacific Fisheries Environmental Laboratories. "Daily Upwelling Indices, 1989-2000." Live Access Server [Website: http://www.pfeg.noaa.gov/products/las.html] Pacific Grove, California.

Peinert, R., et al., 1989. Food web structure and loss rate. W.H. Berger, V.S. Smetacek, Wefer (Eds.). In: Productivity of the ocean; Present and past. Dahlem workshop reports 44, 35-48.

Pennington, J.T., Chavez F.P., 2000. Seasonal fluctuations of temperature, salinity, nitrate, chlorophyll and primary production at station H3/M1 over 1989-1996 in Monterey Bay, California, Deep Sea Research Part II: Topical Studies in Oceanography 47 (5-6), 947-973.

Pilskaln, C.H., Paduan, J.B., Chavez, F.P., Anderson, R.Y., Berelson, W.M., 1996. Carbon export and regeneration in the coastal upwelling system of Monterey Bay, central California. Journal Marine Research 54, 1149-1178.

Riley, G.A., 1946. Factors controlling phytoplankton populations on Georges Bank. Journal Marine Research 6, 54-73.

Riley, G.A., 1947. A theoretical analysis of the phytoplankton populations on Georges Bank. Journal Marine Research 6, 104-113.

Sarmiento, J.L., Slater, R.D., Fasham, M.J.R., Ducklow, H.W., Toggweiler, J.R., Evans, G.T., 1993. A seasonal three-dimensional ecosystem model of nitrogen cycling in the north Atlantic euphotic zone. Global Biogeochemical Cycles 7, 417-450.

Schrader, G.C., 1981. Seasonal Cycles of Phytoplankton in Relation to the Hydrography of Monterey Bay. California State University and Colleges, Moss Landing Marine Laboratories Technical Publication, 81-82.

Service, S.K., Rice, J.A., Chavez, F.P., 1998. Relationship between physical and biological variables during the upwelling period in Monterey Bay CA. Deep Sea Research II 45, 1669-1685.

Silver, M.W., Davoll, P.J., 1975. California Cooperative Fisheries Investigations, plankton data report, Monterey Bay, July 1974 to July 1975. University of California, Santa Cruz, Coastal Marine Laboratory. Technical Report, No. 2. 88.

Silver, M.W., Davoll, P.J., 1976. California Cooperative Fisheries Investigations, plankton data report, Monterey Bay, July 1975 to July 1976. University of California, Santa Cruz, Coastal Marine Laboratory. Technical Report, No. 5. 169.

Silver, M.W., Davoll, P.J., 1977. California Cooperative Fisheries Investigations, plankton data report, Monterey Bay, July 1976 to June 1977. University of California, Santa Cruz, Coastal Marine Laboratory. Technical Report, No. 8. 95.

Simpson, J.J., 1984. El Niño-induced onshore transport in the California current during 1982-1983, Geophysical Research Letter 11, 241-242.

Skogsberg, T., 1936. Hydrography of Monterey Bay, California. Thermal conditions, 1929-1933. Transactions of the American Philosophical Society 29, 1-152.

Skogsberg, T., Phelps, A., 1946. Hydrography of Monterey Bay, California. Thermal conditions, Part II, 1934-1937. Proceedings of the American Philosophical Society 90, 350-386.

Smetacek, V., 1985. The annual cycle of Kiel bight plankton - a long term analysis. Estuaries 8, 145-157.

Smith, R.L., 1995. The physical processes of coastal ocean upwelling systems. In: Summerhayes, C.P., Emeis, K.-C., Angel, M.V., Smith, R.L., Zeitzschel, B. (Eds.), Upwelling in the Ocean: Modern Processes and Ancient Records. Wiley, New York. 39-64.

Strub, P.T., Allen, J.S., Huyer, A., Smith, R.L., 1987a. Large-scale structure of the spring transition in the coastal ocean of western North America. Journal Geophysical Research 92, 1527-1544.

Strub, P.T., Allen, J.S., Huyer, A., Smith, R.L., Beardsely, R.C., 1987b. Seasonal cycles of currents, temperatures, winds, and sea level over the northeast Pacific continental shelf. Journal Geophysical Research 92, 1507-1527.

Strub, P.T., Kosro, P.M., Huyer, A., 1991. The nature of the cold filaments in the California Current System. Journal Geophysical Research 96, 14743-14768.

Stuart, V., 1986. Feeding and metabolism of *Euphausia lucens* (Euphausiacea) in the southern Benguela current. Marine Ecology 30, 117-125.

Summerhayes, C.P., Emeis, K.-C., Angel, M.V., Smith, R.L., Zeitzschel, B., 1995. Upwelling in the Ocean: Modern processes and Ancient Records. Summerhayes, C.P., Emeis, K.-C., Angel, M.V., Smith, R.L., Zeitzschel, B. (Eds.). In: Upwelling in the Ocean: Modern Processes and Ancient Records. Wiley, New York. 2-37.

Takeda, S., 1998. Influence of iron availability on nutrient consumption ratio of diatoms in oceanic waters. Nature 393: 774-776.

Taylor, A.H., Geider, R.J., Gilbert, F.J.H., 1997. Seasonal and latitudinal dependencies of phytoplankton carbon-to-chlorophyll a ratios: results of a modeling study. Marine Ecology Progress Series 152, 51-66.

Toggweiler, J.R., Carson, S., 1995. What are upwelling systems contributing to the ocean's carbon and nutrient budgets? Summerhayes, C. P., Emeis, K.-C., Angel, M. V., Smith, R. L., Zeitzschel, B. (Eds.). In: Upwelling in the Ocean: Modern Processes and Ancient Records. Wiley, New York. 337-360.

Wefer, G., 1989. Particle flux in the ocean: effects of episodic production. Berger, W.H., Smetacek, V.S., Wefer, G. (Eds.). In: Productivity of the ocean; Present and past. Dahlem workshop reports 44, 85-98.

Wheeler, P.A., Kokkinakis, S.A., 1990. Ammonium limits nitrate use in the oceanic subarctic Pacific. Limnology and Oceanography 35, 1267-1278.

Wilkerson, F.P., Dugdale, R.C., Kudela, R.M., Chavez, F.P., 2000. Biomass and productivity in Monterey Bay, California: contribution of the large phytoplankton Deep Sea Research Part II: Topical Studies in Oceanography 47 (5-6), 1003-1022.

APPENDIX: STELLA nine-component model figure

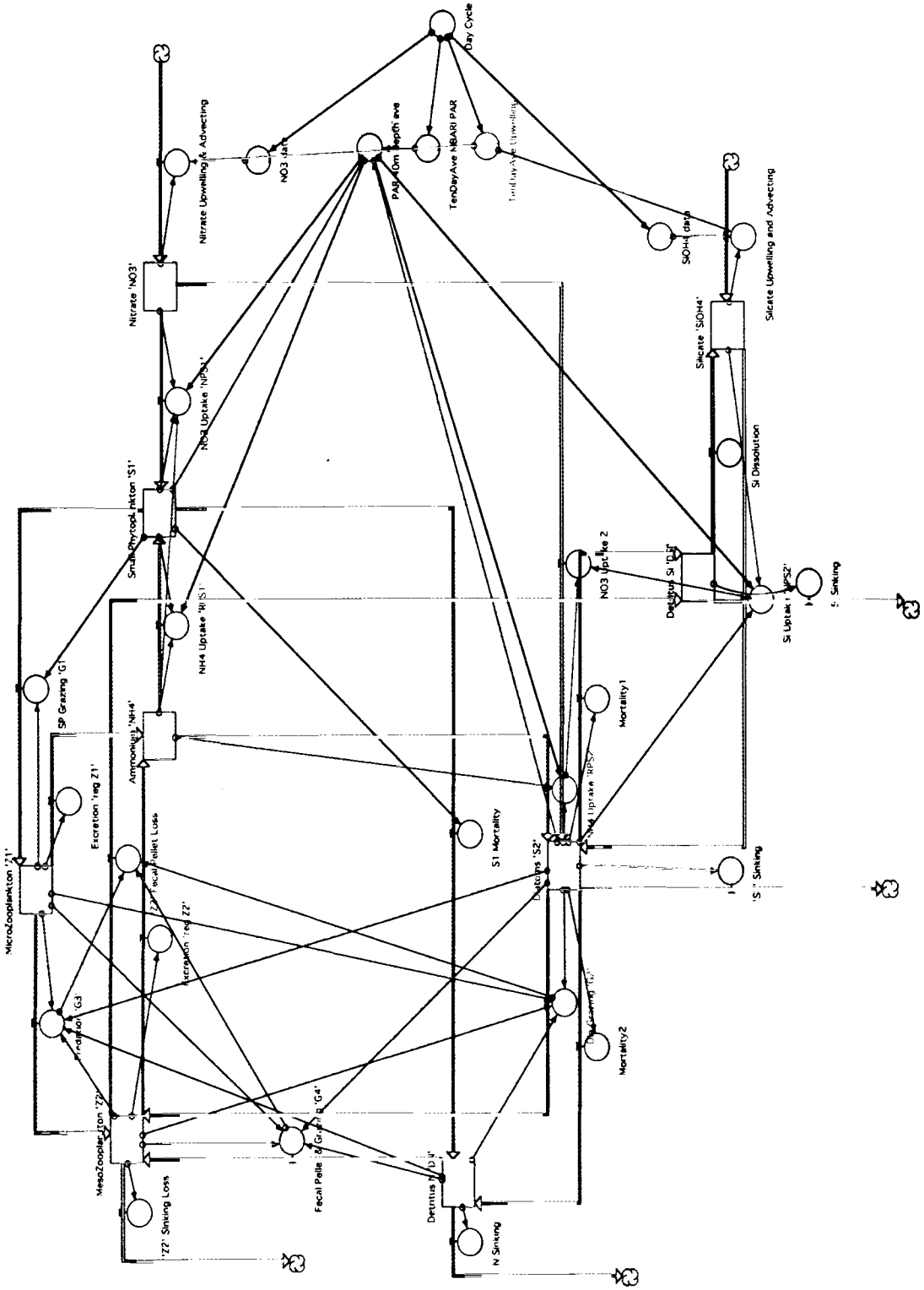

Figure A.1. STELLA nine-component model

BIOGRAPHY OF THE AUTHOR

Lawrence Klein was born in Seattle, Washington, on October 16, 1975. He was raised on Mercer Island, Washington, and graduated from Lakeside School, as a lifer (5^{th}-12^{th} grade), in 1994. He attended Middlebury College, in Vermont, and studied abroad his junior spring semester in New Zealand at the University of Otago, in Dunedin, New Zealand. Lawrence returned his senior year and produced a thesis, titled, *Effects of the Internal Seiche in the South Main Lake of Lake Champlain, Vermont,* in partial fulfillment of the requirements of a B.A. in the department of Geology. After graduating from Middlebury College in 1998, and undertaking a summer internship in Key Largo, at the Marine Resource Development Foundation, Lawrence entered a one-year traveling marine biology program through Northeastern University.

After moving to Maine to attend University of Maine's M.S. program, Lawrence worked as a Chemistry and Oceanography laboratory instructor at the Maine Maritime Academy in Castine, Maine. Lawrence also spent the summer of 2000 at the Monterey Bay Aquarium Research Institute (MBARI) in California as a research assistant, where he gained valuable knowledge, insight, and techniques, for his thesis topic. Lawrence is a candidate for the Master of Science degree in Oceanography from the University of Maine in August, 2002.